COMPARATIVE STUDY OF ACCELERATING AND DECELERATING CORONAL MASS EJECTIONS (CMEs) DURING SOLAR CYCLES 23 AND 24.

ABSTRACT

The behavior of Coronal Mass Ejections (CMEs) across Solar Cycles (SCs) 23 and 24 is investigated, with emphasis on accelerating and decelerating CMEs and their relationships with solar activity indicators such as sunspot area (SSA) and sunspot number (SSN). CMEs, consisting of vast ejections of plasma and magnetic fields, are key contributors to space weather disruptions. Key CME parameters, - Linear Speed (LS), Speed at 20 solar radii (20R), Mass (M), Angular Width (AW), and Kinetic Energy (KE) - were obtained from the LASCO CME Catalogue. At the same time, SSA and SSN were sourced from NASA's OMNI Web Service Archive. Statistical analysis time series, distribution plots, and simple linear regression were used to comparatively analyze accelerating and decelerating CMEs in SCs 23 and 24. Average values of the LS of decelerated CMEs were greater than those of accelerated CMEs with SC 23 exhibiting higher values than SC 24. Average speeds at 20R were higher for accelerated than decelerated CMEs. The average M and KE of decelerated and accelerated CMEs showed similar values for both SCs. In contrast, the average AW of CMEs showed that decelerated CMEs exhibit larger widths than accelerated CMEs. Results show that CME parameters exhibit varied correlations with SSA (in the Northern and Southern Hemispheres) and SSN in SCs 23 and 24. Similarly, the parameters accelerated and decelerated of CMEs showed varied correlations with one another in both SCs. We believe this study will help improve the understanding of CME propagation dynamics and support more accurate predictions of their space weather impacts, enhancing solar-terrestrial models.

Keywords: Coronal Mass Ejections (CMEs), solar activity, sunspot, solar cycle, and geomagnetic storm.

1 INTRODUCTION

The Sun undergoes alternating quiet and active phases. During quiet phases, it emits solar wind into the interplanetary (IP) medium (Kahler, 1987), whereas active phases result in explosive events like solar flares and Coronal Mass Ejections (CMEs). CMEs, the most energetic ejections, carry masses of 10^{13}–10^{16} kg (Georgoulis et al., 2000) with velocities ranging from 100 km/s to 2000 km/s (Hundhausen, 1999). When CMEs with southward magnetic fields reach Earth, they can disrupt power grids, telecommunications, and satellites, and pose risks to astronauts (Silwal et al., 2021; Uga et al., 2024).

Sunspot number (SSN) and sunspot area (SSA) are key indicators of solar activity, reflecting magnetic field dynamics in the Sun's convection zone (Solanki, 2003). During increased solar activity, the emergence and reconnection of magnetic fields often trigger solar flares and CMEs (Gautam et al., 2022, 2024).

Ambient solar wind conditions influence CME propagation. Fast CMEs, primarily driven by Lorentz forces (Forbes, 2000), decelerate beyond 20 solar radii (20R) due to aerodynamic drag. In contrast, slow CMEs accelerate as they interact with the solar wind (Cargill, 2004).

CMEs are categorized based on their kinematic behavior—whether they accelerate, decelerate, or maintain a constant velocity—during their journey through the solar corona and interplanetary space, with this classification determined through detailed observations from solar and space-based observatories. Accelerating CMEs, typically originating from regions of low-speed solar wind or the lower corona, gain velocity as they propagate outward from the Sun, often starting with speeds of 400 km/s or less; their acceleration is largely attributed to magnetic reconnection or Lorentz forces, which propel them until they reach a terminal velocity where outward and resistive forces are balanced. In contrast, decelerating CMEs, which usually begin with high initial speeds of 1000 km/s or more, experience a loss in velocity as they interact with the slower ambient solar wind, where drag forces and the velocity difference between the CME and the surrounding solar wind create opposing forces that slow them down (Sheeley et al., 1999; Cargill, 2004; Gopalswamy & Yashiro, 2005; Vršnak & Žic, 2007).

The statistical analysis of accelerating and decelerating CMEs has been extensively studied to understand their kinematics and variability. Sheeley et al. (1999) identified that decelerating CMEs, typically associated with high initial speeds (≥1000 km/s), experience drag forces as they interact with the slower ambient solar wind, resulting in a gradual loss of velocity. Their analysis for earlier solar cycles showed that these high-speed CMEs often occur during peak solar activity. Gopalswamy and Yashiro (2005) expanded this understanding, demonstrating that accelerating CMEs, originating from low-speed solar wind regions, are influenced significantly by Lorentz forces and magnetic reconnection. These CMEs often exhibit low initial speeds (≤400 km/s) and are more frequent during declining phases of solar activity. Vršnak and Žic (2007) quantified the drag experienced by decelerating CMEs, deriving drag coefficients, and examining their dependence on solar wind density and CME velocity. Their findings reinforced that the velocity difference between the CME and the surrounding solar wind significantly determines the deceleration rate. The studies did not focus on comparing characteristics of solar cycles 23 and 24 which have been reported as periods of high solar activity during solar cycle 23 and periods of low solar activity during solar cycle 24 (Clette & Lefèvre, 2013; Pesnell, 2016; Golpalswamy et al. 2018)

Onuchukwu and Umuogbana (2024) conducted a comprehensive analysis of CME datasets for solar cycles (SC) 23 and 24, focusing on the behavior of accelerating and decelerating CMEs across these cycles. By averaging CME parameters over 27-day solar rotations, as defined by Bartels rotations (Bartels, 1934), the study explored the variability and behavior of CMEs concerning solar activity indicators such as the sunspot number (SSN) and sunspot area (SSA). Their findings aim to refine CME propagation models and improve space weather predictions, crucial for developing effective mitigation strategies for disruptions caused by CME-driven space weather events.

2 DATA COLLECTION AND SOURCES

We analyzed CME data from SCs 23 (August 1996 – March 2008) and 24 (December 2008 – December 2019). SSA and SSN data were obtained from the OMNI Web Service Archive (NASA SPDF - https://omniweb.gsfc.nasa.gov/). CME parameters were extracted from the LASCO CME Catalogue (SOHO -https://cdaw.gsfc.nasa.gov/CME_list/), including:

- Linear Speed (LS): Outward velocity (km/s).
- Speed at 20 solar radii: 20R (km/s).
- Angular Width (AW)
- Mass (M): Estimated using white-light coronagraph images (Howard and Tappin, 2009) and Kinetic Energy (KE).

We selected all the CMEs classified as accelerating ((Accel) 19 178) or decelerating (Decel) 13 297) and divided them into two subsamples for each SC. In SC 23, we have 8 369 CMEs classified as accelerating and 6 595 CMEs classified as decelerating. In SC 24, we have 10 809 CMEs classified as accelerating and 6 702 CMEs classified as decelerating.

3 **DATA ANALYSIS**

For the subsamples (accelerated and decelerated), we obtained the 27-day mean and median values, which we used in the scatter and distribution plots. We also obtained the yearly averages, which we used in the time series plots.

We analyzed yearly averaged means, medians, and 27-day averages of CME parameters to assess their variability across SCs 23 and 24. Histogram distributions were utilized to examine the parameter distributions, focusing on skewness and kurtosis. To investigate the relationships between parameters and their connection to solar activity, we generated scatter plots of 27-day averages of CME parameters against one another and calculated correlation coefficients for CME parameters in relation to sunspot number (SSN) and sunspot area (SSA).

Our analysis incorporated both the mean and the median, each offering distinct advantages and limitations as measures of central tendency in statistical evaluation. The mean provides a complete representation of the dataset by incorporating every data point, making it especially useful when all values hold equal significance. It effectively captures overall trends by considering all data, offering a comprehensive view of fluctuations over time (Chen et al., 2020; Hamilton, 1994), and represents the true central tendency in cases of symmetrical data distribution without outliers. However, the mean is highly sensitive to outliers or extreme values, which can distort its accuracy, leading to misleading trends in visualizations of time series data (Rousseeuw & Leroy, 2003). Moreover, it may not accurately represent datasets with seasonal spikes or irregular patterns, as the averaging process tends to smooth out critical short-term deviations.

On the other hand, the median is robust against outliers, making it a better measure of central tendency for skewed or non-normal distributions. It provides a clearer representation of typical behavior in datasets with irregular spikes or extreme values (Wilcox, 2017), offering an accurate depiction of central trends without being influenced by extreme fluctuations (Koenker, 2005). Despite these strengths, the median has limitations: it does not reflect the spread or variability of data, potentially overlooking volatility patterns (Witten et al., 2016). Additionally, calculating the median for large or real-time datasets can be computationally intensive compared to the mean.

Furthermore, the median is less applicable in statistical models or calculations requiring a mean, such as standard deviation or correlation analysis (Chatfield, 2003).

4.1 ANALYSIS ON MONTHLY SUNSPOT AREA

Fig 1 depicts the SSN variations observed during SCs 23 and 24. Notably, these sunspot numbers exhibit a distinctive double-hump pattern, a phenomenon previously documented by Ramesh and Rohini (2010). The double hump for SC 23 is not unusual, as it is typically noticed in odd-numbered SCs (Bazilevskaya et al., 2000). A comparative analysis of the highest peaks in SSNs clearly illustrates the relative feebleness of SC 24 and its less symmetric pattern compared to its predecessor, SC 23 (Petrovay 2020). The extent of this SC's weakness is unprecedented in the history of the space age, as pointed out by Singh and Bhargawa (2017).
Fig 1 also displays the monthly SSA plot for SCs 23 and 24, aiming to analyze and compare the SSA in the Northern Hemisphere (SSANH) and the SSA in the Southern Hemisphere (SSASH) for both SCs. The solar variation shows peak events in the years 2000 and 2014 for SCs 23 and 24, respectively. The peak SSA for both hemispheres is generally higher for SC 23 compared to SC 24, indicating a relative weakness in SC 24. However, the asymmetry between the Northern and Southern Hemispheres is more pronounced in SC24 compared to SC23. This increased mismatch in SC 24 supports the observation of its overall reduced activity (Chowdhury et al., 2013; Li et al., 2008). Interestingly, signs of weakening were already noticeable in SC 23, leading some scientists to suggest that we may be approaching another Maunder Minimum, a period of significantly reduced solar activity (Singh & Bhargawa, 2017; Petrovay, 2020).

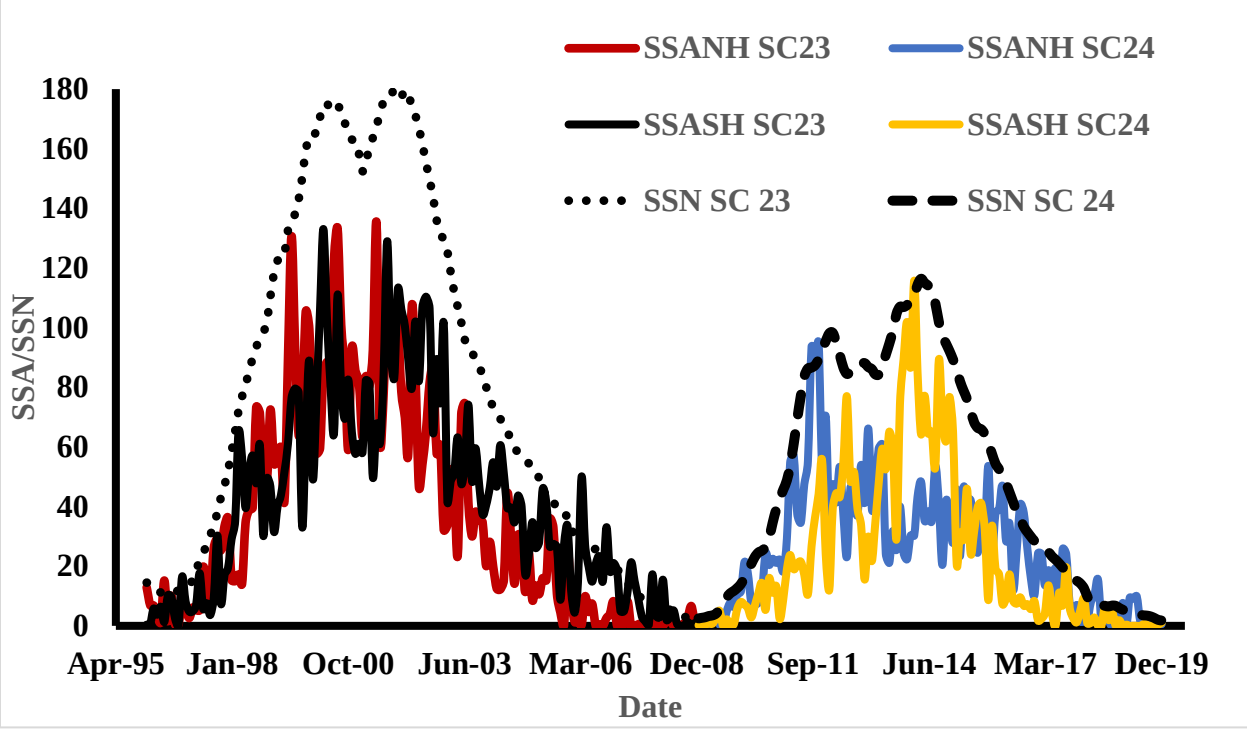

Fig 1: Monthly averaged Sunspot Number and Sunspot Area time series (see Onuchukwu & Umuogbana, 2024)

4.2 ANALYSIS ON MEAN AND MEDIAN TIME SERIES FOR ACCELERATING AND DECELERATING CMEs

The yearly averaged CPA for accelerating and decelerating CMEs (Fig 2a) displays notable differences across SCs 23 and 24. For accelerating CMEs in SC 23, the mean CPA shows variability with peaks reaching up to 240°, whereas in SC 24, the mean exhibits higher variability but lower overall peaks, reflecting a less consistent pattern. Decelerating CMEs in SC 23 also show fluctuating mean CPA values, generally hovering around 200°. In SC 24, the mean CPA of decelerating CMEs displays even greater variability, indicating a broader range of ejection CPA compared to SC 23, likely influenced by the weaker solar magnetic fields during the cycle.

The median CPA for accelerating CMEs in SC 23 (Fig 2b) remains relatively stable around 180°, showing less variability compared to the mean. In SC 24, the median CPA for accelerating CMEs follows a similar trend but displays reduced stability, diverging slightly more from the mean. For decelerating CMEs, the median CPA in SC 23 fluctuates around 200° but is generally more consistent than in SC 24. In SC 24, the median CPA shows a significant divergence from the mean, reflecting a less uniform distribution of ejection directions. These trends corroborate findings by Vourlidas et al. (2010) and Webb et al. (2000), which highlight the variability of CPA influenced by solar magnetic conditions across cycles.

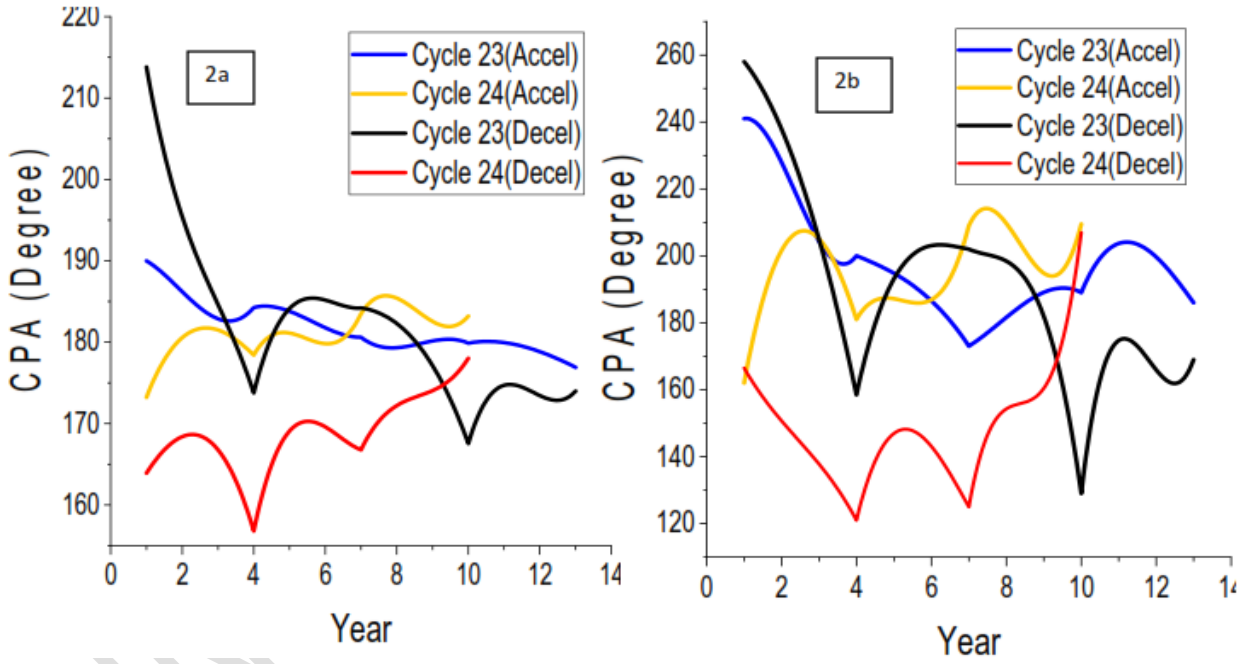

Fig. 2 Yearly Mean and Median Time Series Plot of the CPA for the Accelerating and Deceleration CMEs during SCs 23 and 24 (2a – Using the Yearly Mean Values; 2b – Using the Yearly Median Values)

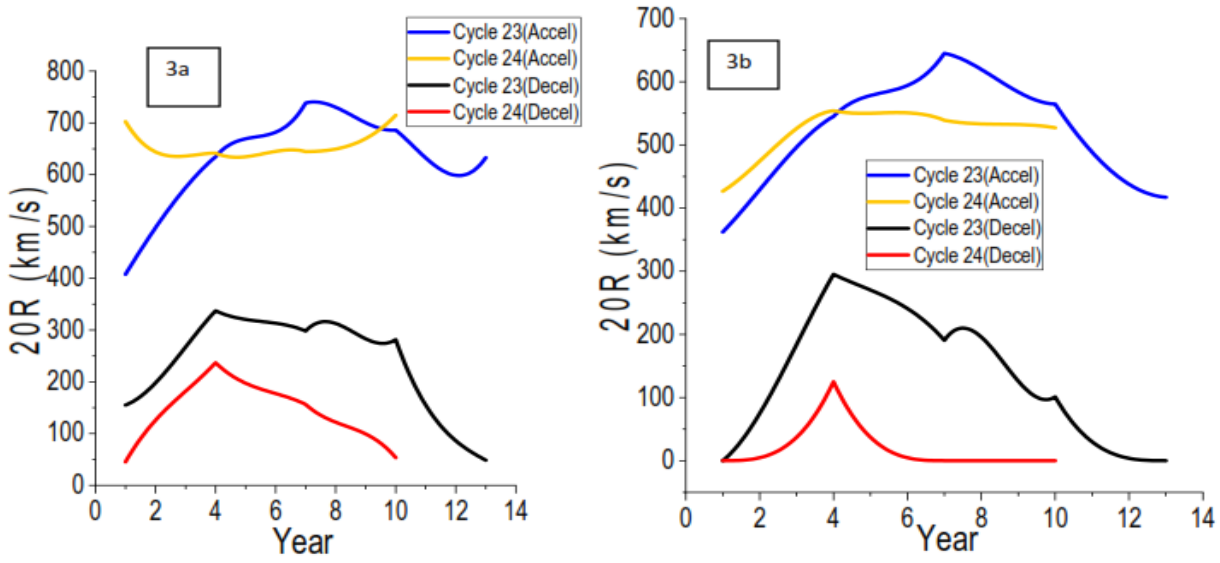

Fig. 3 Yearly Mean and Median Time Series Plot of the 20R for the Accelerating and Deceleration CMEs during SCs 23 and 24 (3a – Using the Yearly Mean Values; 3b – Using the Yearly Median Values)

The yearly averaged mean speeds at 20R of accelerating CMEs (Fig. 3a) are consistently higher than those of decelerating CMEs across both SC 23 and SC 24. In SC 23, accelerating CMEs reach a peak mean speed of approximately 700 km/s around year 7, while decelerating CMEs peak early in the cycle and gradually decline, with mean speeds not exceeding 500 km/s. Similarly, in SC 24, the mean speed of accelerating CMEs peaks at around 600 km/s in year 8, while decelerating CMEs show significantly lower mean speeds, remaining below 300 km/s throughout the cycle. These trends highlight the stronger influence of solar activity on the propagation dynamics of accelerating CMEs compared to decelerating CMEs (Gopalswamy et al., 2001; Zhang et al., 2004)

The median speeds of accelerating CMEs (Fig. 3b) also surpass those of decelerating CMEs across both cycles but are consistently lower than their corresponding mean speeds, reflecting the influence of high-speed outliers. In SC 23, accelerating CMEs exhibit a median speed peak around year 7, closely following the mean trend but at reduced values. Decelerating CMEs in SC 23 show a gradual decline in median speeds, with values remaining significantly lower than their mean counterparts. In SC 24, both accelerating and decelerating CMEs display subdued median speeds, with accelerating CMEs peaking below 600 km/s and decelerating CMEs showing even lower values, indicating a more pronounced deceleration in the weaker solar cycle. This differentiation between median and mean speeds underscores the variability and outlier influence, particularly for accelerating CMEs during active phases of SC 23 (Gopalswamy et al., 2001; Zhang et al., 2004).

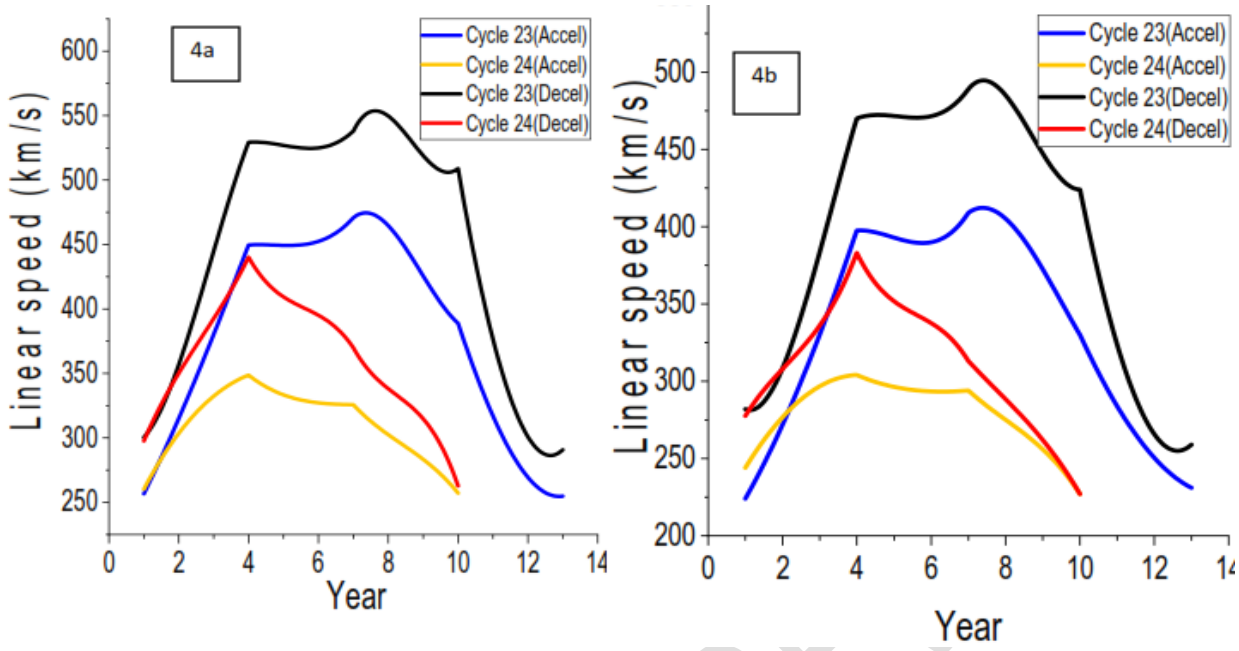

Fig. 4 Yearly Mean and Median Time Series Plot of the LS for the Accelerating and Deceleration CMEs during SCs 23 and 24 (4a – Using the Yearly Mean Values; 4b – Using the Yearly Median Values)

The yearly averaged mean LS (4a) for accelerating CMEs in SC 23 is consistently higher than those in SC 24. In SC 23, the mean speed reaches up to approximately 500 km/s, while in SC 24, the mean speed peaks around 400 km/s, indicating a notable reduction in speed during the weaker solar activity of SC 24. For decelerating CMEs, SC 23 also exhibits higher mean speeds, with a pronounced peak around the mid-cycle years reaching 500 km/s, whereas SC 24 shows significantly lower mean speeds, peaking at around 400 km/s. These trends corroborate findings by Youssef (2012) and Gopalswamy et al. (2001), which suggest that CMEs exhibit higher speeds during periods of intense solar activity, aligning with the stronger solar maximum of SC 23.

The median LS for both accelerating and decelerating CMEs follows a similar trend, with SC 23 consistently showing higher values than SC 24. For accelerating CMEs, the median speed in SC 23 closely follows the mean, peaking slightly below 500 km/s, while in SC 24, it remains lower, with peaks around 400 km/s. Similarly, for decelerating CMEs, the median speed in SC 23 shows a pronounced mid-cycle peak, remaining slightly below the mean, whereas SC 24 exhibits subdued peaks around 400 km/s. These differences in median LS further highlight the influence of reduced solar activity in SC 24, leading to overall lower CME speeds compared to SC 23.

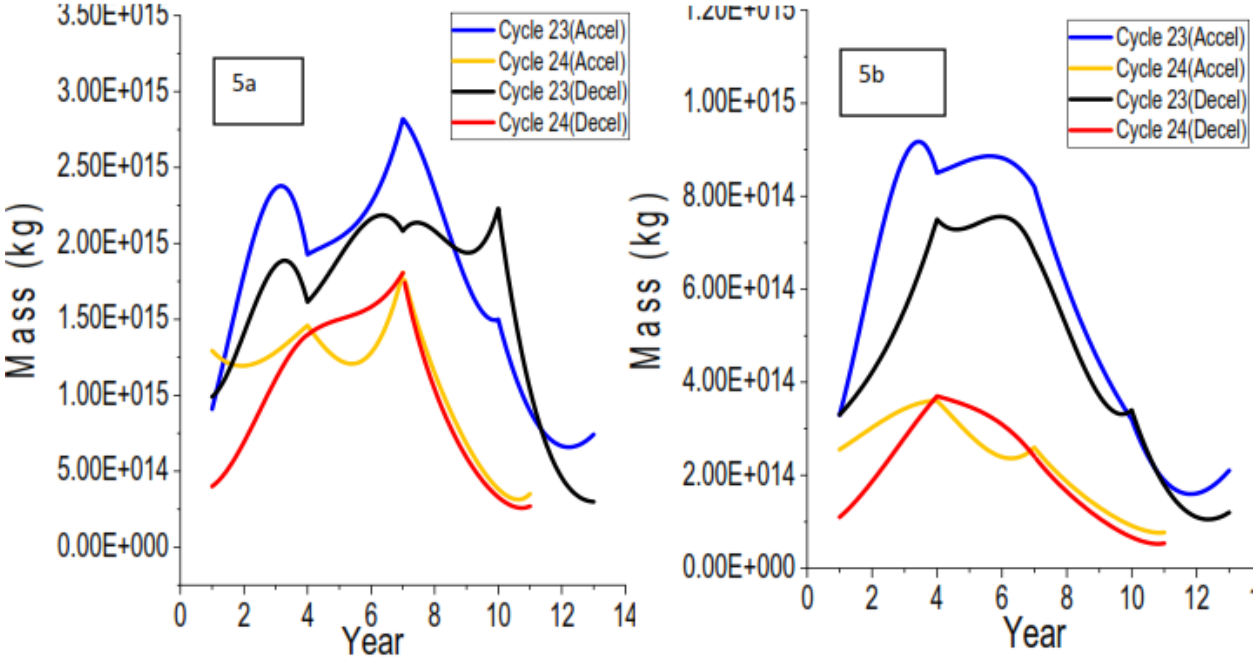

Fig. 5 Yearly Mean and Median Time Series Plot of the Mass for the Accelerating and Deceleration CMEs during SCs 23 and 24 (5a – Using the Yearly Mean Values; 5b – Using the Yearly Median Values)

The yearly averaged mean masses of accelerating CMEs (5a) show significant differences between SC 23 and 24. In SC 23, the mean mass peaks around 8.0×10^{15} kg during the 4th and 8th years, reflecting substantial variability, while in SC 24, the mean mass shows a declining trend after an initial peak, reaching around 2.0×10^{15} kg. For decelerating CMEs, SC 23 also demonstrates higher mean masses, with peaks up to approximately 2.0×10^{15} kg, whereas SC 24 exhibits lower values, peaking at about 1.5×10^{15} kg. These differences align with observations by Webb & Howard (2012) and Vourlidas et al. (2010), which link higher CME masses to periods of intense solar activity, consistent with the stronger solar maximum of SC 23.

The median masses of accelerating CMEs (5b) are generally lower but follow similar trends across the solar cycles. In SC 23, the median mass remains relatively stable around 10^{15} kg, while in SC 24, it is reduced, hovering around 4.0×10^{14} kg For decelerating CMEs, SC 23 shows noticeable peaks in median mass during the early to mid-cycle years, though the values remain lower than the mean. In SC 24, the median masses are significantly subdued, with much lower peak values compared to SC 23. These trends further emphasize the reduced solar activity and lower mass ejections in SC 24 relative to SC 23.

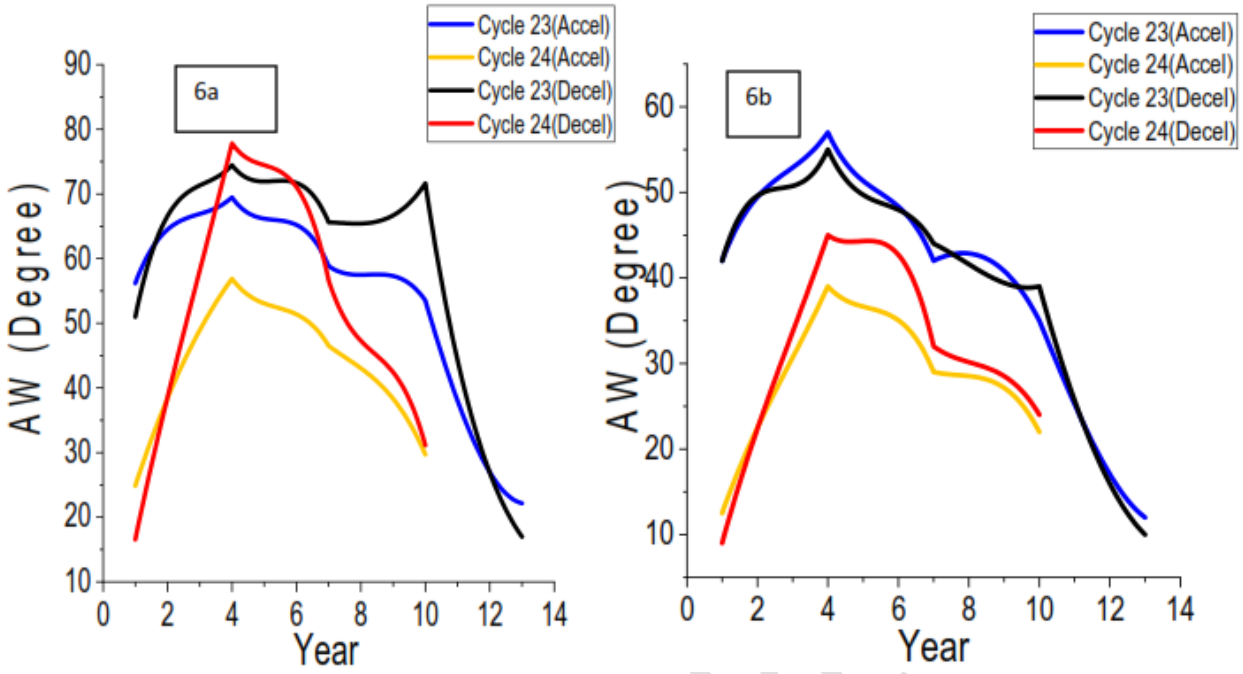

Fig. 6 Yearly Mean and Median Time Series Plot of the Mass for the Accelerating and Deceleration CMEs during SCs 23 and 24 (6a – Using the Yearly Mean Values; 6b – Using the Yearly Median Values)

The yearly averaged mean AW of accelerating and decelerating CMEs (Fig 6a) show distinct patterns across SCs 23 and 24. In SC 23, the mean AW for accelerating CMEs peaks earlier, around years 4-5, and is generally higher than that of decelerating CMEs, which peaks later at the mid-cycle. In SC 24, both accelerating and decelerating CMEs exhibit lower and more subdued mean AW values, with the accelerating CMEs maintaining a slight edge over the decelerating ones. These differences highlight the influence of solar activity, with SC 23's higher solar activity producing more extreme events.

The median AW for accelerating CMEs in SC 23 is consistently lower than the mean but follows a similar trend (Fig 6b), peaking earlier in the cycle. For decelerating CMEs, the median AW in SC 23 peaks slightly later but remains lower than that of accelerating CMEs. In SC 24, both accelerating and decelerating CMEs display reduced median AW values, with minimal variation. The smaller difference between median and mean values in SC 24 suggests fewer extreme events, further underscoring the reduced solar activity of the cycle.

The yearly averaged KE of accelerating and decelerating CMEs (Fig 7a) highlights significant differences across SCs 23 and 24. For accelerating CMEs, the mean KE peaks sharply during the early to middle years of SC 23, indicating the presence of several very energetic events that elevate the average. Decelerating CMEs in SC 23 also exhibit higher mean KE values, with pronounced peaks reflecting the cycle's overall higher solar activity. In SC 24, both accelerating and decelerating CMEs show significantly lower mean KE values, with fewer and smaller peaks, underscoring the reduced solar activity and fewer high-energy events during this cycle.

The KE for accelerating CMEs in SC 23 follows a similar trend to the mean but remains consistently lower (Fig7b), reflecting the influence of a few highly energetic events skewing the mean upwards. For decelerating CMEs, the median KE in SC 23 also peaks but stays below that of accelerating CMEs. In SC 24, the median KE for both accelerating and decelerating CMEs is closer to the mean, indicating less variability and fewer extreme events. These trends further emphasize the quieter and less dynamic nature of SC 24 compared to the energetic environment of SC 23.

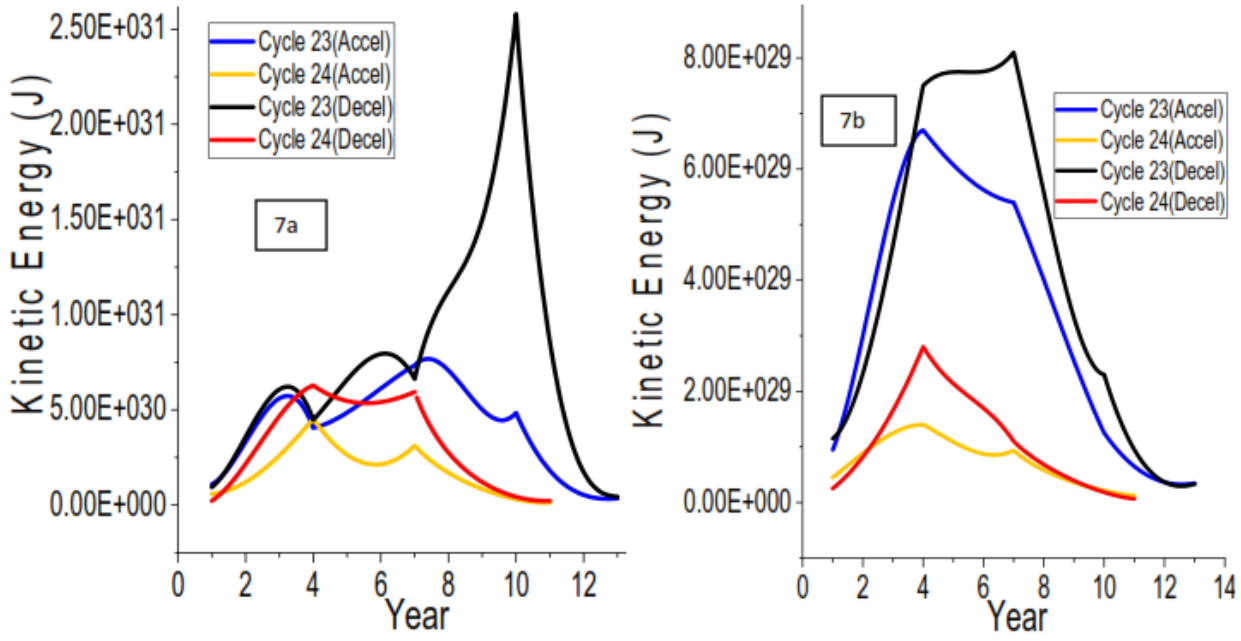

Fig. 7 Yearly Mean and Median Time Series Plot of the Mass for the Accelerating and Deceleration CMEs during SCs 23 and 24 (7a – Using the Yearly Mean Values; 7b – Using the Yearly Median Values)

Table 1 shows the average yearly mean and median values of the accelerated and decelerated CME parameters. The range of the mean and median values of the CPA are similar for accelerated CMEs for SC 23 and 24. Still, for decelerated CMEs, the mean and median values of CPA for SC 23 were generally higher than for SC 24. The mean and median values of the linear speed of accelerated CMEs were lower than that of decelerated CMEs. The linear speed of accelerating CMEs is typically lower than that of decelerating CMEs due to differences in their initial driving forces, ambient solar wind conditions, and the physics of propagation in the solar corona and interplanetary medium. Accelerating CMEs often originate from regions with weaker initial driving forces, such as low-energy magnetic reconnections or gradual eruptions in the solar corona. They start with relatively low speeds, typically in the range of 100–400 km/s (Gopalswamy & Yashiro, 2005). The magnetic forces in the lower corona gradually act on these CME until it reaches a balance with the drag force from the solar wind (Cargill, 2004). These accelerating CMEs often propagate in regions with faster solar wind, where the velocity gradient (difference between the CME and solar wind speeds) is smaller, reducing the drag force and allowing gradual acceleration.

TABLE 1: TABLE OF STATISTICS OF CME PARAMETERS FOR ACCELERATED AND DECELERATED CMEs

Decelerating CMEs typically begin with high speeds, often exceeding 1000 km/s, driven by explosive magnetic reconnection events like those associated with X-class flares or fast streamer blowouts (Vršnak, 2001). This results in relatively slower terminal velocities. These decelerating

PARAMETERS	Mean (Accelerated CMEs)	Median (Accelerated CMEs)	Mean (Decelerated CMEs)	Median (Decelerated CMEs)
SC 23 CPA (deg)	180.9 ± 23.2	197.1	181.4 ± 27.0	187.1
SC 24 CPA (deg)	181.5 ± 27.4	195.2	169.8 ± 29.3	152.2
SC 23 LS (km/s)	384.5 ± 106.4	345.3	476.1 ± 138.1	377.5
SC 24 LS (km/s)	315.2 ± 52.3	284.3	436.0 ± 122.7	319.5
SC 2320R (km/s)	652.2 ± 138.1	531.2	260.3 ± 136.0	169.6
SC 24 20R (km/s)	649.4 ± 99.9	535.1	161.7 ± 89.4	92.3
SC 23 MASS (kg) $\times 10^{15}$	15.1 ± 0.4	14.7	15.1 ± 0.5	14.7
SC 24 MASS (kg)$\times 10^{15}$	14.9 ± 0.3	14.4	15.1 ± 0.4	14.8
SC 23 KE (J) $\times 10^{30}$	30.1 ± 0.7	29.4	30.4 ± 0.8	29.6
SC 24 KE (J) $\times 10^{30}$	29.9 ± 0.6	28.9	30.2 ± 0.7	29.1
SC 23 AW (deg)	52.4 ± 21.4	40.5	61.4 ± 26.5	41.5
SC 24 AW (deg)	46.3 ± 14.3	30.7	60.4 ± 27.1	36.5

CMEs are driven by powerful eruptions that impart high initial kinetic energy, allowing them to overcome solar wind resistance initially. However, as they travel into the slower ambient solar wind, the drag force causes them to decelerate. It has been noted that high-speed CMEs propagate through slower solar wind, creating a large velocity gradient that results in significant drag and deceleration (Vršnak & Žic, 2007).

Accelerating CMEs are often powered by weaker or prolonged energy release mechanisms, whereas decelerating CMEs are linked to intense and sudden energy releases, giving them higher initial velocities (Sheeley et al., 1999). The linear speed difference arises because accelerating CMEs have weaker initial impulses and rely on external forces (e.g., magnetic reconnection) for gradual acceleration, whereas decelerating CMEs start with a high kinetic energy that diminishes over time due to drag forces in the solar wind. The mean and median values of speed at 20R of accelerated CMEs were higher than those of decelerated CMEs. SC 23 being more active has a higher average linear speed and speed at 20R for both accelerated and decelerated CMEs than SC 24.

The mass of accelerating CMEs and decelerating CMEs is often similar because both involve large-scale ejections of plasma from the Sun. Our mean and median values are shown in Table 2 for decelerating and accelerating CMEs for SCs 23 and 24 (see Table 2). The mass is typically determined by the density of the plasma in the solar corona and the volume of the ejected material. However, CMEs associated with intense solar events, such as flares or active region eruptions, often have slightly higher masses (decelerating CMEs) due to the larger-scale magnetic reconnection processes involved (Gopalswamy et al., 2009). The kinetic energy of decelerating

CMEs is significantly higher than that of accelerating CMEs. This is because kinetic energy depends on both mass and the square of velocity. CME mass is primarily governed by the plasma density in the corona and the volume of ejected material. While there can be variations, the difference between accelerating and decelerating CMEs is not as significant as their kinetic energy (Vourlidas et al., 2010).

Decelerating CMEs typically start with very high velocities (≥1000 km/s) due to explosive magnetic reconnection, resulting in higher kinetic energy. Accelerating CMEs, starting at lower velocities (≤400 km/s), have much lower initial kinetic energy (Vršnak, 2001). The higher velocities of decelerating CMEs, driven by explosive processes like intense solar flares, amplify their kinetic energy compared to accelerating CMEs, which gradually gain speed under weaker forces (Cargill, 2004). In Table 2, the average kinetic energy we estimated for SCs 23 and 24 for accelerating and decelerating CMEs were similar perhaps due to decelerating CMEs losing speed while accelerating CMEs gaining speed.

Generally, the AW of CME during SC 23 was larger than in SC 24, but decelerated CMEs have larger angular widths than accelerated CMEs. Several works e.g. Schwenn et al., (2005), Gopalswamy et al., (2006), Zhang & Dere, (2006), Lugaz et al., (2012), and Möstl et al., (2012), have concluded that accelerated CMEs gain speed as they propagate through the corona and interplanetary space, thus, they tend to have narrower angular widths. Decelerated CMEs lose speed as they propagate, often due to interactions with the ambient solar wind or other CMEs, thus they tend to have broader angular widths, as they interact more strongly with the surrounding solar wind, causing them to expand and increase their angular width. Furthermore, decelerated CMEs may undergo magnetic reconnection, leading to a broader angular width as the CME's magnetic field lines are reconfigured.

4.3 DISTRIBUTION PLOTS

The histogram of the mean Central Position Angle (CPA) for accelerating and decelerating CMEs reveals distinct patterns across SCs 23 and 24 (Fig 8). For accelerating CMEs in SC 23, the mean CPA is centered around 160°–180°, with a relatively symmetric distribution and a slight positive skew, indicating most CMEs are concentrated around these central values with fewer events at higher CPAs. In SC 24, the mean CPA for accelerating CMEs shifts slightly higher and displays a broader distribution, reflecting greater variability in the central positions. Similarly, for decelerating CMEs, SC 23 exhibits a more symmetric distribution centered around 170°, while SC 24 shows broader variability, with the mean CPA peaking slightly higher around 180°, indicating an increased range of ejection directions during SC 24. These trends are consistent with findings by Cremades and Bothmer (2004) and Youssef (2012), which highlight the role of solar magnetic field dynamics in shaping CPA distributions across cycles.

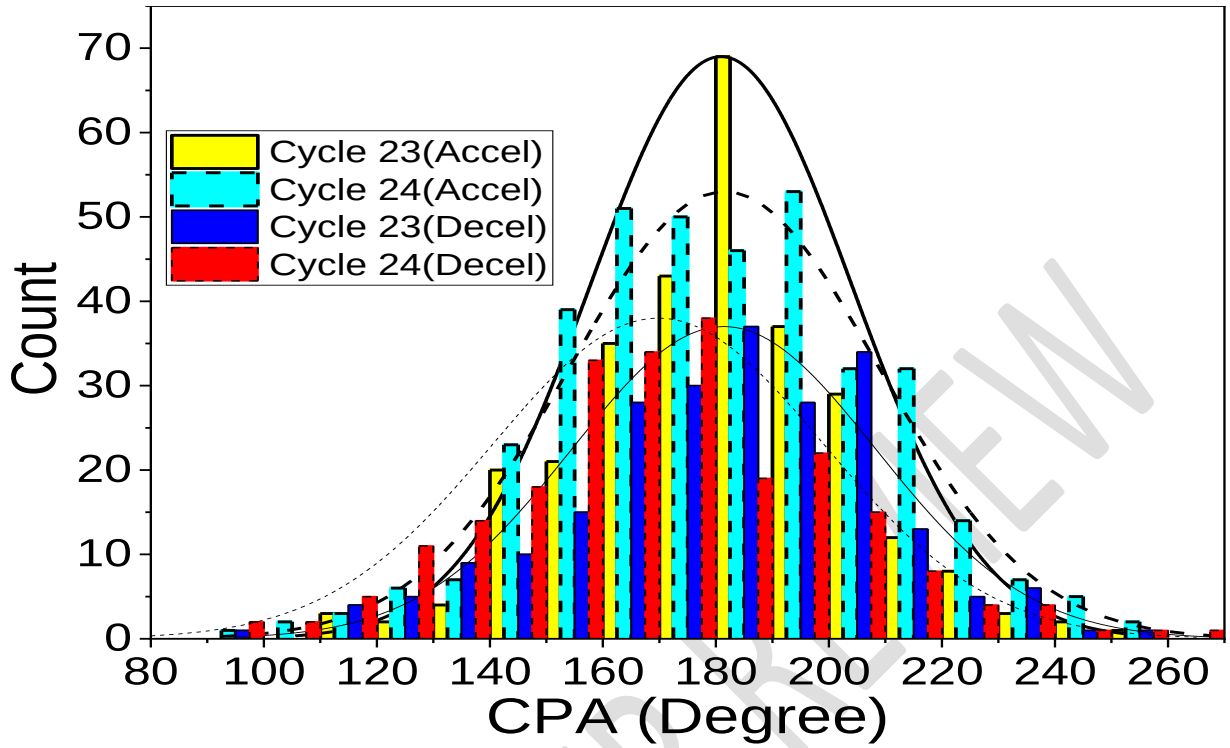

Fig. 8. Distribution Plot of CPA using the 27-day Mean Values for Accelerating and Deceleration CMEs during SCs 23 and 24

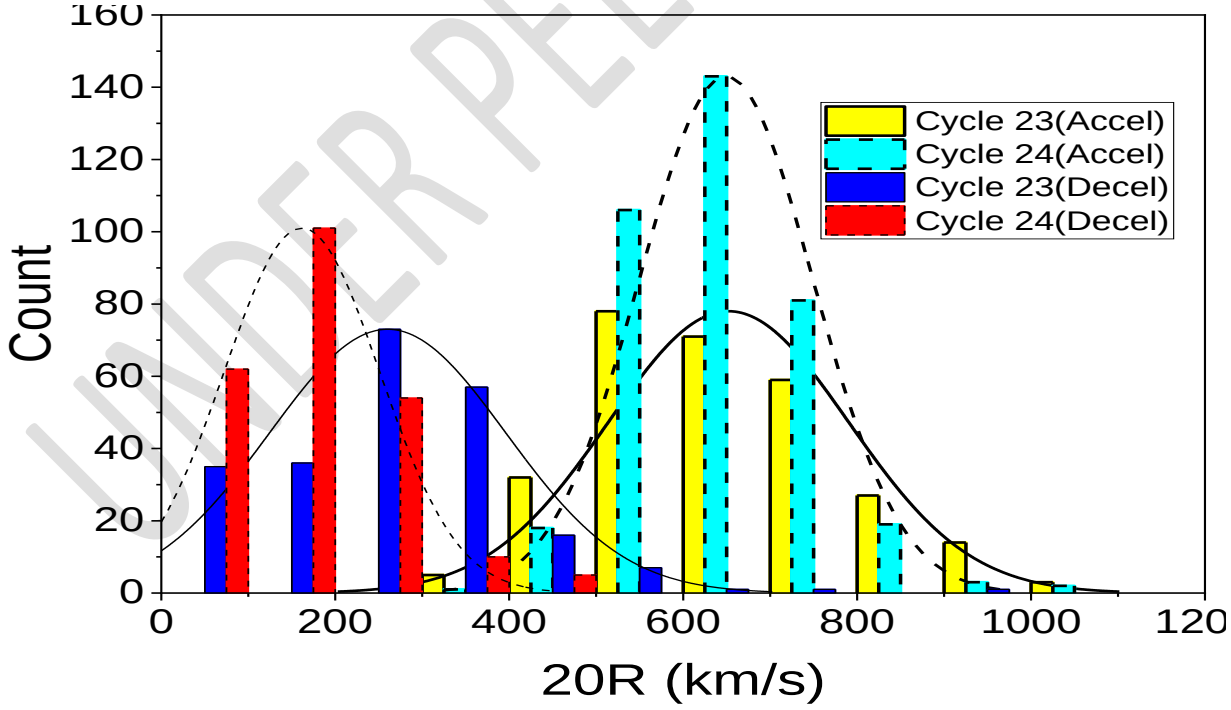

Fig. 9. Distribution Plot of 20R using the 27-day Mean Values for Accelerating and Deceleration CMEs during SCs 23 and 24

The mean speed at 20R for accelerating CMEs in SC 23 peaks around 400−500 km/s, while for decelerating CMEs, it is significantly lower, peaking at 200−300 km/s (Fig. 9) at large distances from the sun. This indicates that accelerating CMEs consistently achieve higher speeds compared to their decelerating counterparts. In SC 24, the mean speed of accelerating CMEs increases, peaking at 500–600 km/s, while the mean speed of decelerating CMEs also rises, reaching 300–400 km/s. Both types of CMEs exhibit broader distributions and higher mean speeds in SC 24, reflecting an increase in faster-propagating CMEs during this cycle, see Schrijver & DeRosa (2003) regarding speed distributions during active cycles.

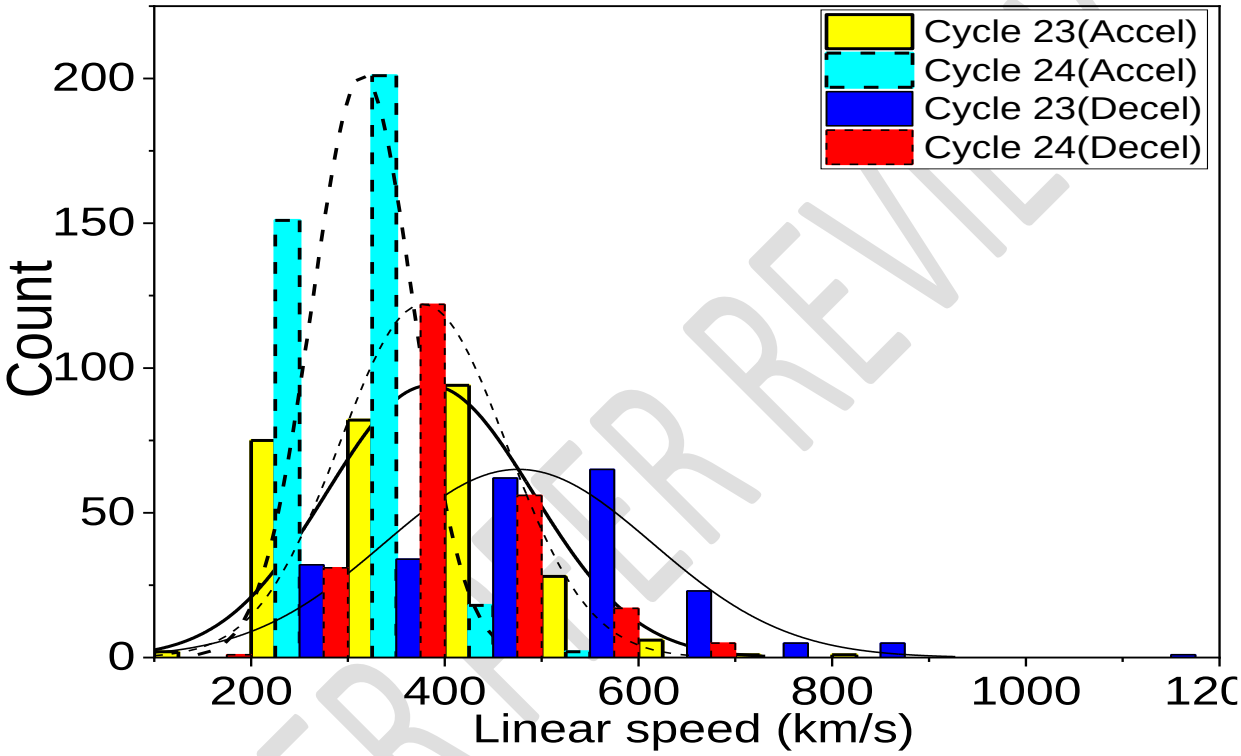

Fig. 10. Distribution Plot of Linear Speed using the 27-day Mean Values for Accelerating and Deceleration CMEs during SCs 23 and 24

The mean linear speed for accelerating CMEs in SC 23 is concentrated around 300–400 km/s, with a peak at approximately 350 km/s, while for decelerating CMEs (Fig 10), the mean follows a similar range with a comparable peak at 350 km/s. Both distributions are slightly positively skewed, indicating the presence of a few very fast CMEs. In SC 24, the mean linear speed for accelerating CMEs increases, peaking at 400–500 km/s, while the mean for decelerating CMEs also rises, with a peak at 400–450 km/s. The broader and higher mean values in SC 23 suggest the presence of more high-speed CMEs, consistent with the findings of Schrijver and DeRosa (2003) and Temmer et al. (2008), which highlight broader and elevated speed distributions during more active cycles.

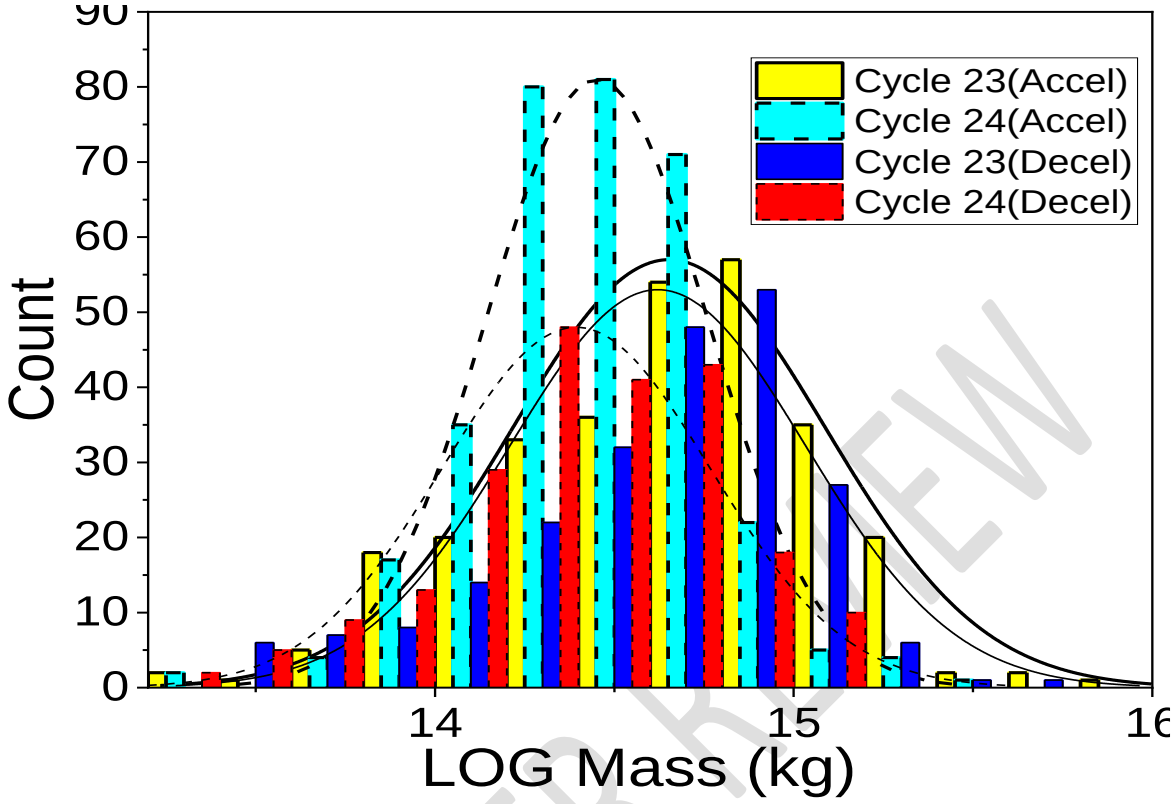

Fig. 11. **Distribution Plot of log Mass using the 27-day Mean Values for Accelerating and Deceleration CMEs during SCs 23 and 24**

The mean mass of accelerating CMEs in SC 23 is concentrated around 10^{14} to 10^{15} kg (Fig 11), with a peak at approximately $10^{14.5}$ kg, exhibiting a relatively symmetric distribution with a slight positive skew due to a few massive events. For decelerating CMEs in SC 23, the mean mass follows a similar pattern, with values also concentrated in the range of 10^{14} to 10^{15} kg and a comparable peak. In SC 24, both accelerating and decelerating CMEs display broader distributions, with slightly higher peaks around 10^{14} kg. The more pronounced positive skew in SC 23 suggests a greater occurrence of massive CMEs during this cycle, consistent with Kahler (2006), who observed that CME mass distributions often exhibit positive skewness during active solar phases.

For accelerating CMEs, the mean AW during SC 23 peaks around 40°–50° (Fig 12), with the distribution showing a relatively sharp decline beyond this range. The overall distribution in SC 23 is narrower, suggesting fewer very wide CMEs. In contrast, SC 24 shows a broader distribution, with the mean AW slightly higher, peaking around 50°–60°. This broader distribution and higher mean in SC 24 reflect the presence of more events with larger angular widths. For decelerating CMEs, SC 23 exhibits a narrower and more symmetric distribution of AW, with the mean concentrated around 30°–40°. SC 24, on the other hand, has a broader range of AW values, with the mean shifted slightly higher, peaking around 40°–50°, similar to the pattern for accelerating CMEs

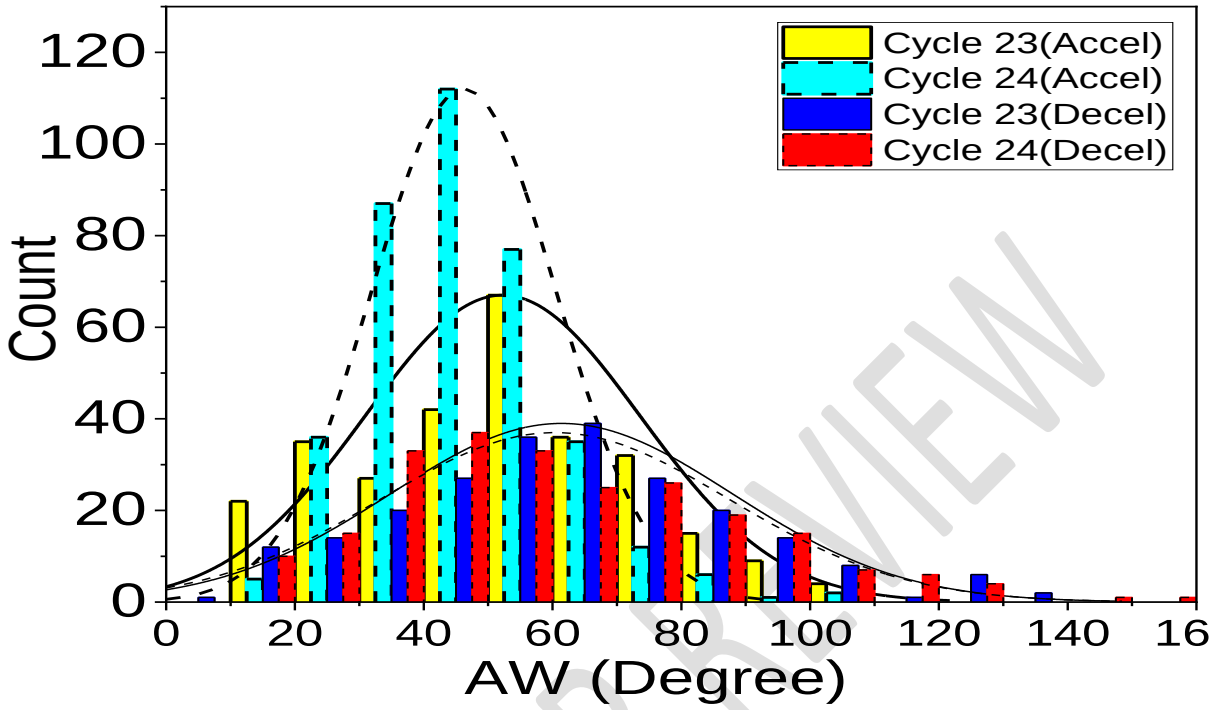

Fig. 12. Distribution Plot of AW using the 27-day Mean Values for Accelerating and Deceleration CMEs during SCs 23 and 24

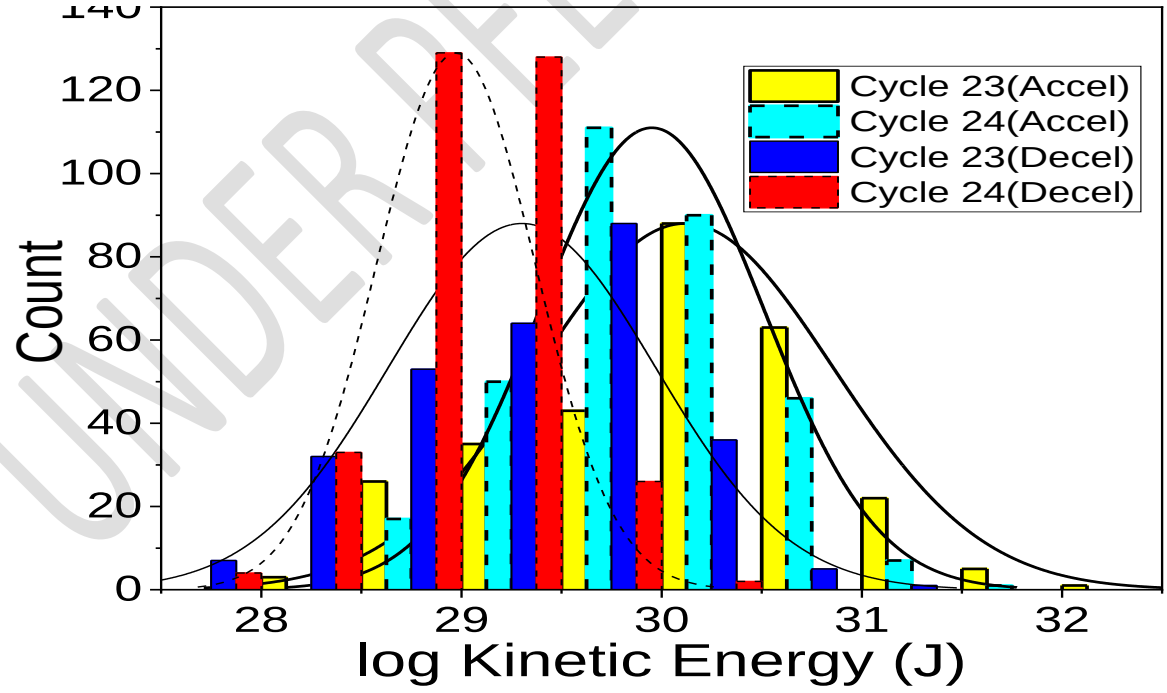

Fig. 13. Distribution Plot of log Kinetic Energy using the 27-day Mean Values for Accelerating and Deceleration CMEs during SCs 23 and 24

The mean kinetic energy of accelerating CMEs shows distinct differences between SC 23 and SC 24. In SC 23, the mean kinetic energy is centered around $10^{29.8}$ J, reflecting moderate energy levels. In contrast, SC 24 exhibits a higher mean of approximately $10^{29.6}$ J, indicating an increase in the energy of CMEs during this cycle. For decelerating CMEs, the mean KE in SC 23 is slightly lower, around $10^{29.6}$ J, same for SC 24, the mean is about $10^{29.4}$ J. These differences underscore that both accelerating have higher energies than decelerating CMEs, while CMEs during SC 23 have higher average energies than SC 24, which aligns with Schrijver and DeRosa (2003), who reported broader distributions and higher CME energies during periods of heightened solar activity.

4.4 Regression Analysis of CME and Solar Activity Parameters.

Table 2: Correlation Coefficients of SSN, SSANH, and SSASH with CMEs Parameters Estimated Using the 27-day mean Values

	Accel	Accel	Decel	Decel
	SC 23	SC 24	SC 23	SC 24
Parameters	r	r	r	r
SSN/LS	0.7	0.6	0.7	0.6
SSANH/LS	0.5	0.6	0.5	0.5
SSASH/LS	0.5	0.5	0.5	0.5
SSN/20R	0.4	-0.2	0.7	0.6
SSANH/20R	0.3	-0.1	0.5	0.5
SSASH/20R	0.4	-0.2	0.4	0.5
SSN/AW	0.5	0.7	0.5	0.8
SSANH/AW	0.4	0.6	0.3	0.6
SSASH/AW	0.1	0.6	0.2	0.8
SSN/M	0.7	0.2	0.6	0.6
SSANH/M	0.5	0.3	0.4	0.5
SSASH/M	0.4	0.1	0.4	0.5
SSN/KE	0.7	0.5	0.6	0.7
SSANH/KE	0.5	0.6	0.4	0.6
SSASH/KE	0.4	0.4	0.4	0.5

Table 2 shows the correlation coefficients of solar activity parameters (SSN, SSANH, and SSASH) with CME parameters for accelerated and decelerated CMEs during SCs 23 and 24. The linear speed showed fairly strong with SSN, SSANH, and SSASH with ≥ 0.5 For the accelerated and decelerated CME parameters for SCs 23 and 24 (see Figs 14-16).

The positive correlation between the linear speed of CMEs and the SSN for accelerated and decelerated CMEs can be attributed to the increased solar activity during periods of higher SSN. The Sun exhibits heightened magnetic activity during solar maxima, characterized by higher SSN. This results in stronger and more complex magnetic fields in the corona. These enhanced fields can influence the dynamics of CMEs, often imparting higher initial energy, which translates to increased linear speeds. Accelerated CMEs are typically associated with active regions that have strong magnetic field gradients and higher solar energetic particle (SEP) events. These conditions

are more prevalent during periods of high SSN, supporting the observed positive correlation. Decelerated CMEs often occur when CMEs interact with the ambient solar wind or interplanetary magnetic field. During high SSN periods, the ambient solar wind is also more turbulent, potentially leading to greater interaction and energy transfer, which can influence the deceleration process. The increased magnetic energy available during periods of high SSN contributes to both the initiation and propagation dynamics of CMEs, affecting their speeds regardless of whether they are accelerated or decelerated (Vršnak, 2001; Gopalswamy & Yashiro, 2006; Chen, 2011).

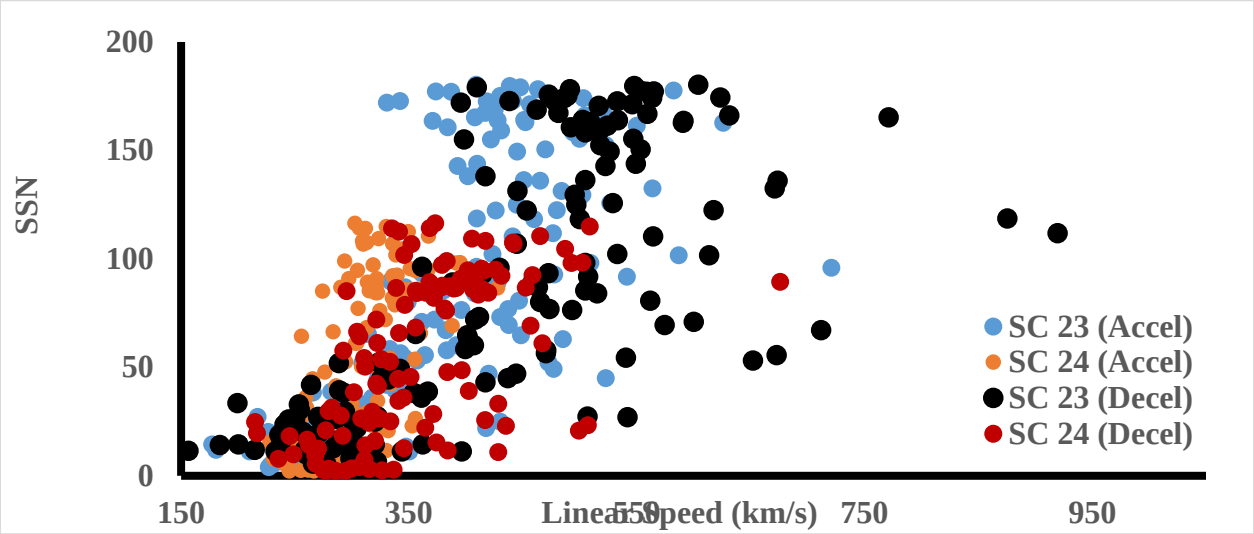

Fig 14: The Scatter Plot of the SSN with Linear Speed for Accelerated and Decelerated CMEs During SC s 23 and 24, Using the 27-day Mean Values

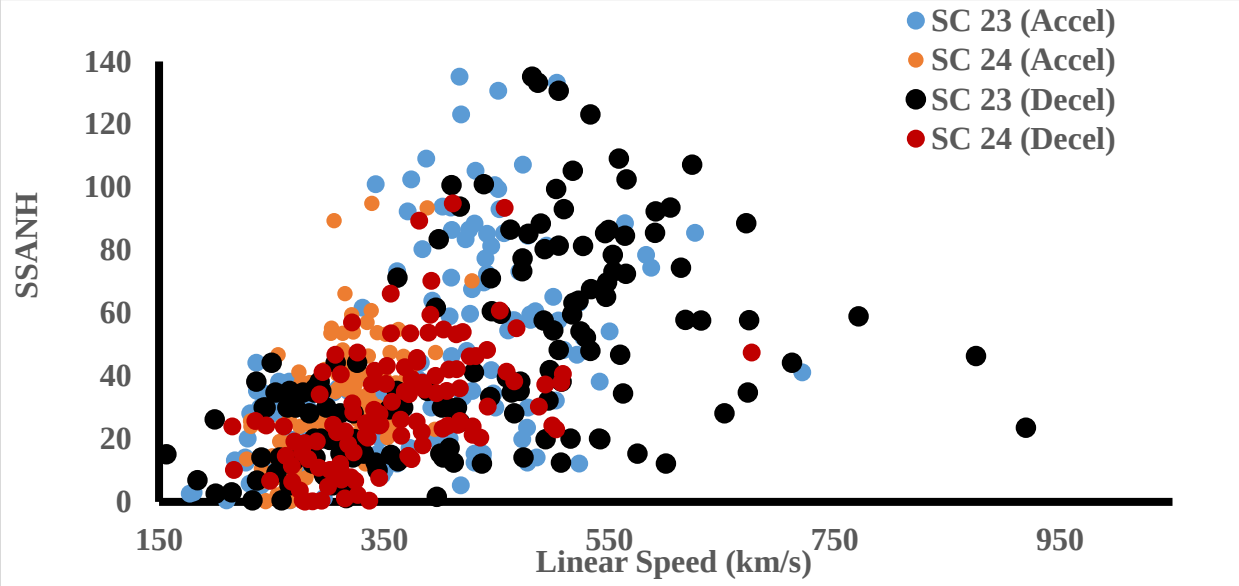

Fig 15: The Scatter Plot of the SSANH with Linear Speed for Accelerated and Decelerated CMEs During SC s 23 and 24, Using the 27-day Mean Values

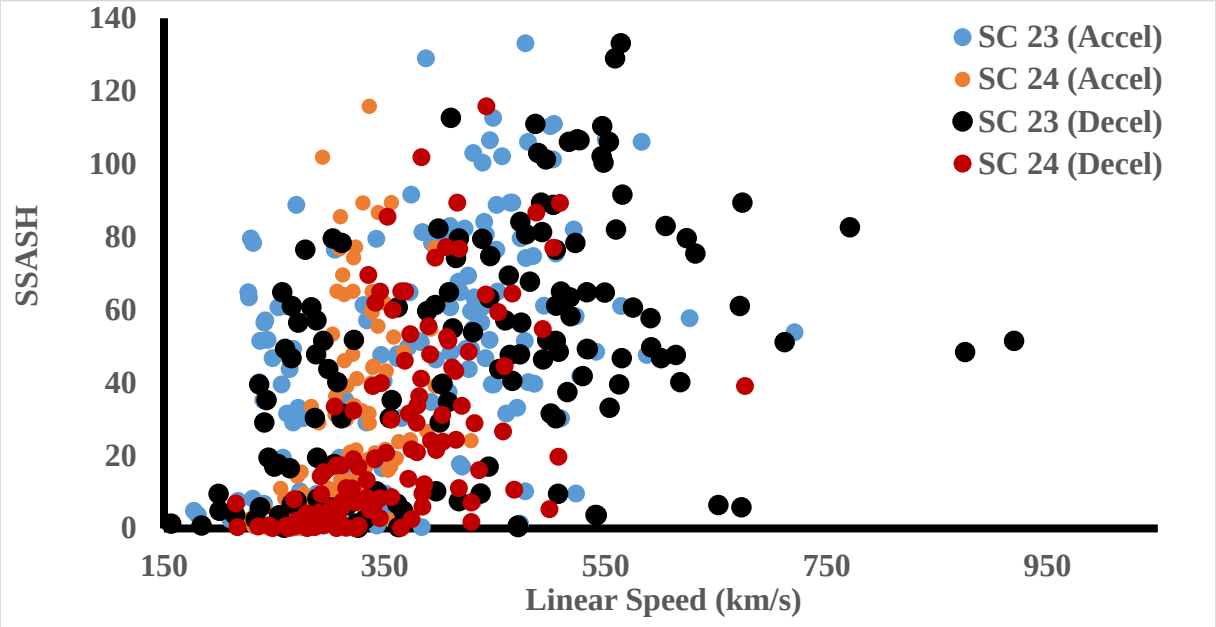

Fig 15: The Scatter Plot of the SSASH with Linear Speed for Accelerated and Decelerated CMEs During SC s 23 and 24, Using the 27-day Mean Values

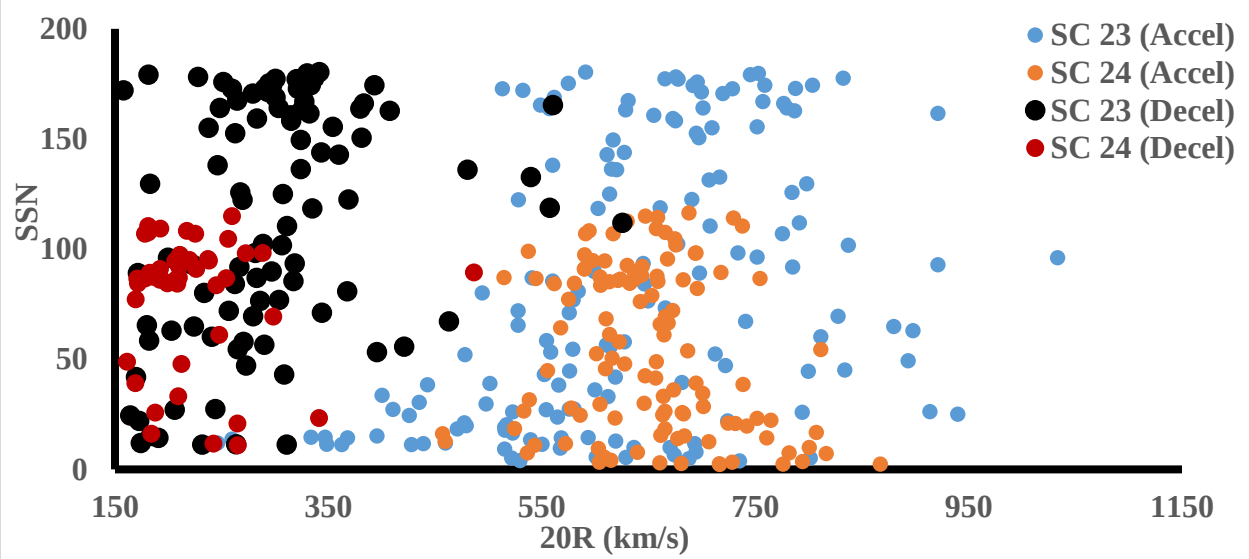

Fig 16: The Scatter Plot of the SSN with speed at 20R for Accelerated and Decelerated CMEs During SC s 23 and 24, Using the 27-day Mean Values

The correlation coefficients presented in Table 2 suggest that SSN are positively correlated with the speed at 20R for accelerated CMEs during SC 23 ($r \approx 0.4$) and decelerated CMEs in SC 23 and 24 ($r \geq 0.6$). However, a weak negative correlation is observed for accelerated CMEs in SC 24 ($r = -0.2$). Similar patterns are evident in the correlations involving sunspot areas in the SSANH and SSASH with speed at 20R. Though Mishra et al. (2019) found an increase in CME activity relative to SSNs in SC 24 compared to SC 23, indicating a change in the relationship between these

parameters, their study is with the whole CMEs, while ours is with a subset (accelerated and decelerated). Thus, this study highlights the need for a detailed study of the various subsets of CMEs to for it will help scientists understand the complexity of solar activities.

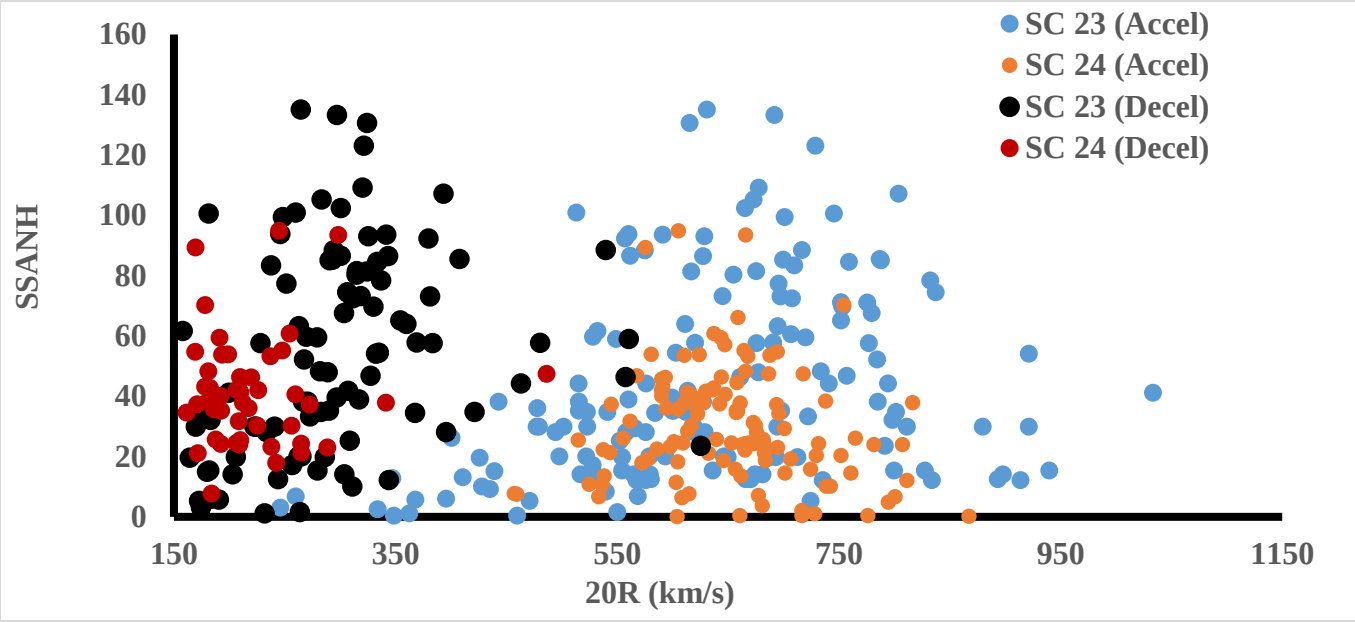

Fig 17: The Scatter Plot of the SSANH with speed at 20R for Accelerated and Decelerated CMEs During SC s 23 and 24, Using the 27-day Mean Values

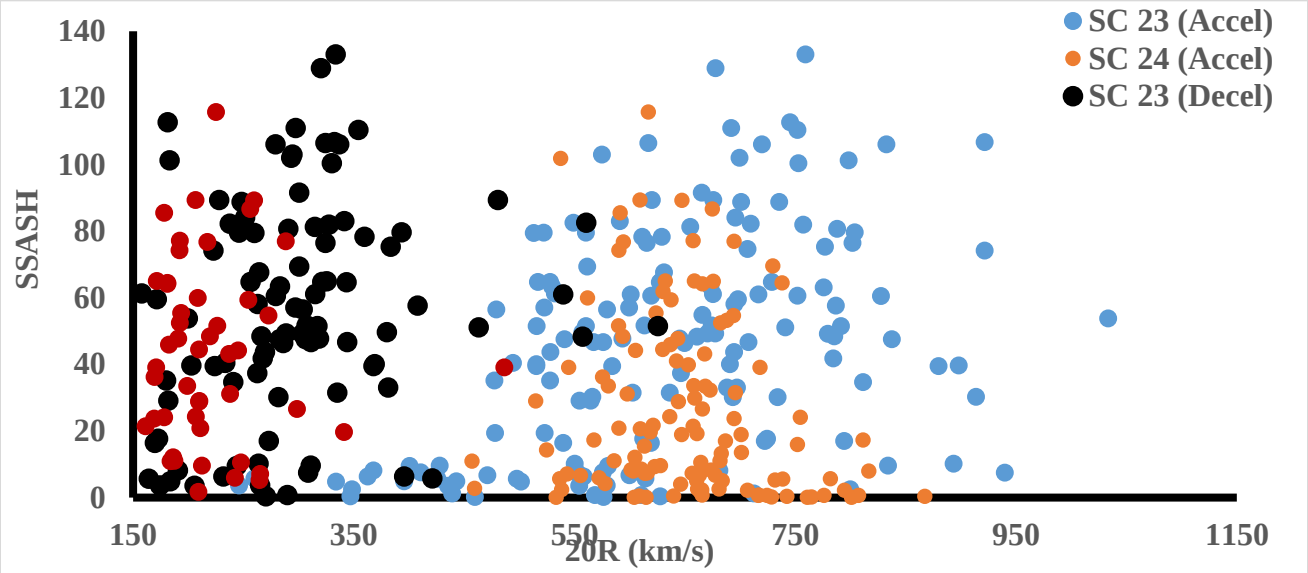

Fig 18: The Scatter Plot of the SSANH with speed at 20R for Accelerated and Decelerated CMEs During SC s 23 and 24, Using the 27-day Mean Values

CMEs are significant expulsions of plasma and magnetic fields from the Sun's corona into the heliosphere. Their kinematic behavior, particularly within 20R from the Sun, is influenced by initial velocities and interactions with the ambient solar wind. CMEs with higher initial velocities often experience deceleration due to aerodynamic drag as they move through the solar wind, which typically has speeds ranging from 100 to 700 km/s within 20R (Sheeley et al., 1997). This deceleration continues until the CME's speed aligns with that of the surrounding solar wind. Conversely, slower CMEs may undergo acceleration, propelled by the solar wind, until their velocities match the ambient flow. This dynamic leads to a convergence of CME speeds toward the solar wind speed as they propagate beyond 20R. Various studies indicate that the most significant acceleration or deceleration of CMEs occurs close to the Sun, typically within 10R, with fast CMEs becoming decelerated between 20 and 50R (Liu et al., 2016; Manchester et al., 2017).

Figs 16 – 18, seem to suggest in general, that accelerated CMEs achieve higher speed at 20R than decelerated CMEs for both SCs, but generally, during SC 23 both decelerated and accelerated CMEs recorded higher speed at 20R than corresponding types in SC 24.

The correlation coefficients in Table 2 showed that SSN, SSANH, and SSASH displayed stronger positive correlations with AW during SC 24 ($r \geq 0.6$) than during SC 23 ($r \leq 0.5$) for both accelerated and decelerated CMEs, particularly in SC 23, AW showed a very weak correlation with SSASH with $r \leq 0.2$ for the accelerated and decelerated CMEs. In Figs 19 – 21, we display the scatter plots of SSN, SSANH, SSASH, and AW for accelerated and decelerated CMEs during SCs 23 and 24.

Research in general indicates a positive correlation between sunspot activity and CME angular width. As sunspot numbers and areas increase, the angular width of CMEs tends to expand. This suggests that more extensive sunspot activity contributes to the development of broader CMEs. While sunspot activity varies between the Northern and Southern Hemispheres, studies have not conclusively demonstrated significant differences in CME angular widths originating from either hemisphere. The relationship between sunspot areas in each hemisphere and CME characteristics remains an area for further investigation. Generally, the distribution of CMEs with varying angular widths does not always align directly with sunspot number variations over time. For instance, CMEs with angular widths between 0° and 60° have exhibited multiple peaks that do not correspond precisely with sunspot number fluctuations, indicating that factors beyond sunspot activity may influence CME angular widths (Du, 2012; Zhang & Liu, 2017). There is a general positive correlation between sunspot numbers and areas with CME angular widths, suggesting that increased sunspot activity leads to broader CMEs. However, the complexities of this relationship, including hemispheric differences and temporal variations, indicate that additional factors contribute to CME characteristics. Further research is necessary to fully understand the interplay between sunspot activity and CME properties (Du, 2012; Li & Luhmann, 2013; Zhang & Liu, 2017).

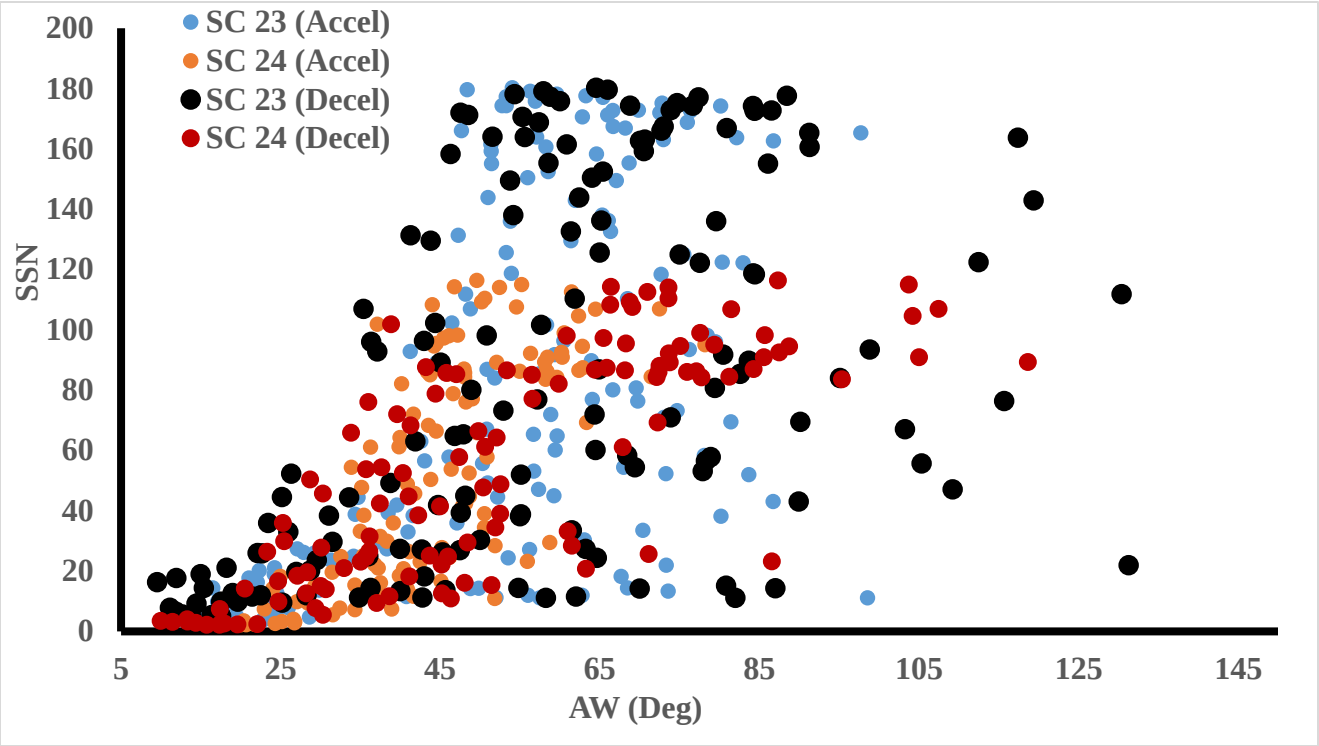

Fig 19: The Scatter Plot of the SSN with speed at 20R for Accelerated and Decelerated CMEs During SC s 23 and 24, Using the 27-day Mean Values

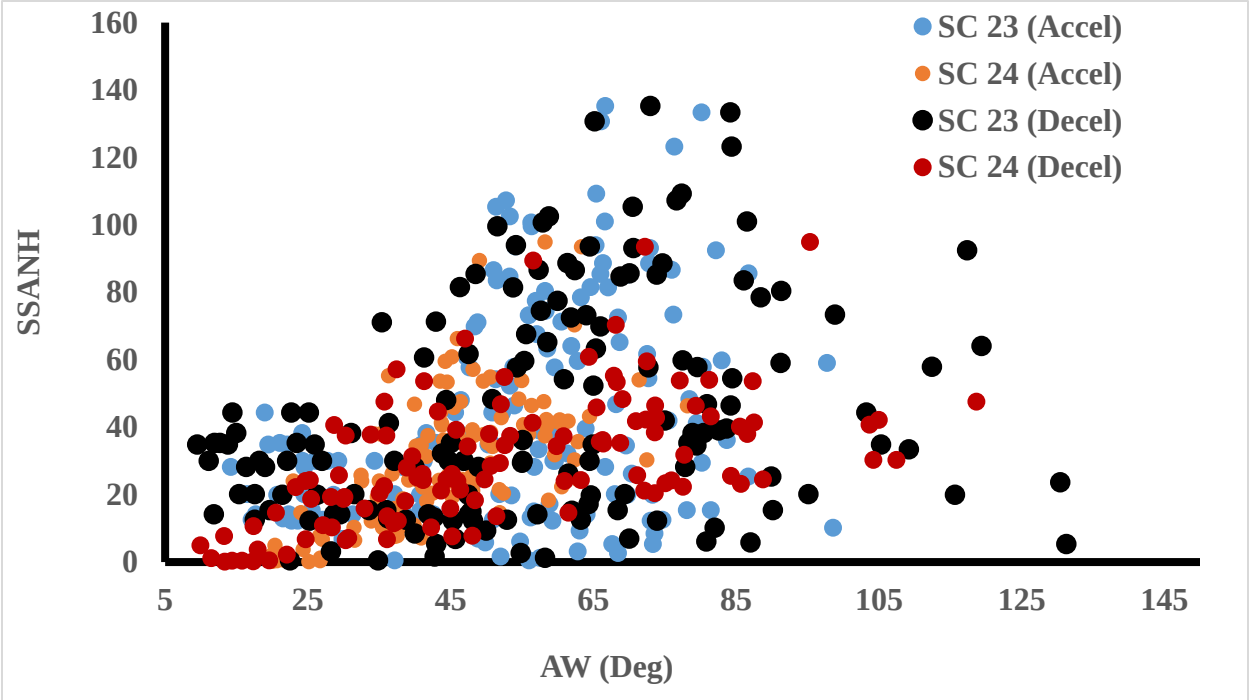

Fig 20: The Scatter Plot of the SSANH with speed at 20R for Accelerated and Decelerated CMEs During SC s 23 and 24, Using the 27-day Mean Values

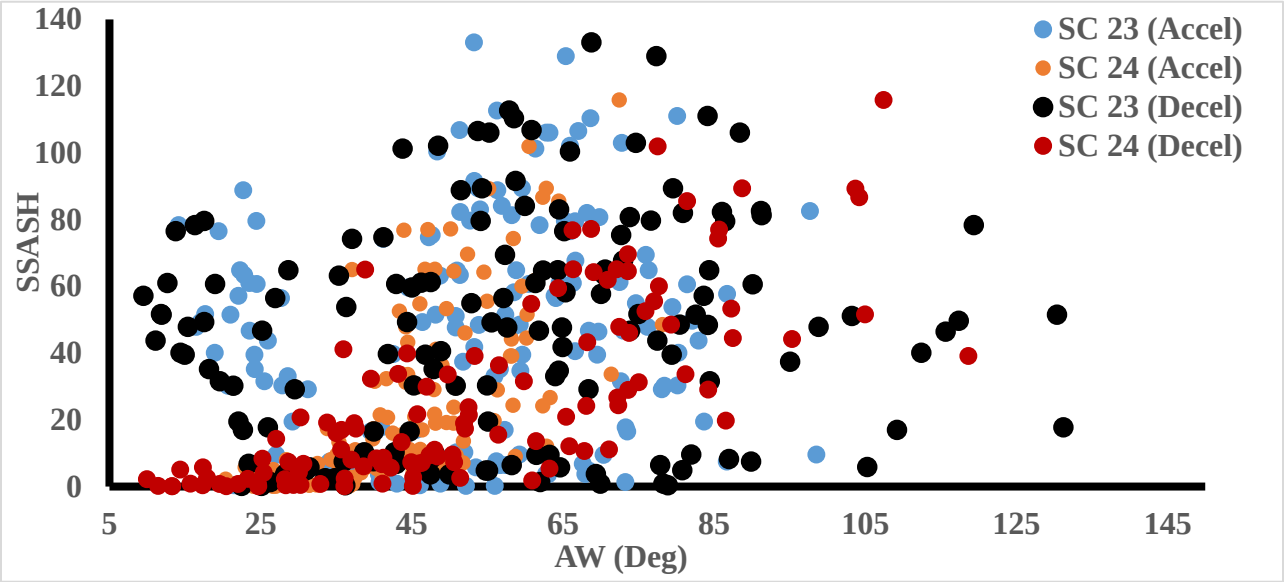

Fig 21: The Scatter Plot of the SSASH with speed at 20R for Accelerated and Decelerated CMEs During SC s 23 and 24, Using the 27-day Mean Values

Correlation coefficient results from Table 2, indicated that solar activity parameters considered in this study corrected positively with the mass and kinetic energy of accelerated and decelerated CMEs for both SCs 23 and 24, with a correlation coefficient $r \geq 0.4$, except for the mass of accelerated CMEs where the correlation coefficient is $r \leq 0.3$ with solar parameters. The relationship between sunspot activity (SSNs and SSAs in the Northern and Southern Hemispheres) and the mass and kinetic energy of CMEs during SCs 23 and 24 has been the subject of extensive research. Studies have demonstrated a positive correlation between sunspot activity and CME properties. Increased SSNs and SSANH/SSASH are associated with a higher frequency of CMEs, as well as greater CME mass and kinetic energy. This trend is evident in both SC 23 and 24, indicating that periods of heightened sunspot activity contribute to more massive and energetic CMEs (Mishra et al., 2019). There exist in the literature studies on the impact of the distribution of sunspot activity between the Northern and Southern Hemispheres and how they can influence CME characteristics. However, the specific impact on the mass and kinetic energy of accelerated and decelerated CMEs requires further investigation, which our study now provides. Comparative analyses of SCs 23 and 24 reveal notable differences in sunspot activity and CME properties. SC 24 exhibited a lower peak in sunspot numbers compared to SC 23, yet the CME occurrence rate and associated mass loss did not decrease proportionally. This discrepancy suggests a complex relationship between sunspot activity and CME characteristics, with factors beyond sunspot numbers influencing CME mass and kinetic energy (Lamy et al., 2019). Our results is in agreement with the study.

The acceleration or deceleration of CMEs is influenced by their interaction with the solar wind and interplanetary magnetic fields. While sunspot activity contributes to the initiation and properties of CMEs, the subsequent kinematic behavior—whether a CME accelerates or decelerates—is determined by external forces encountered during propagation

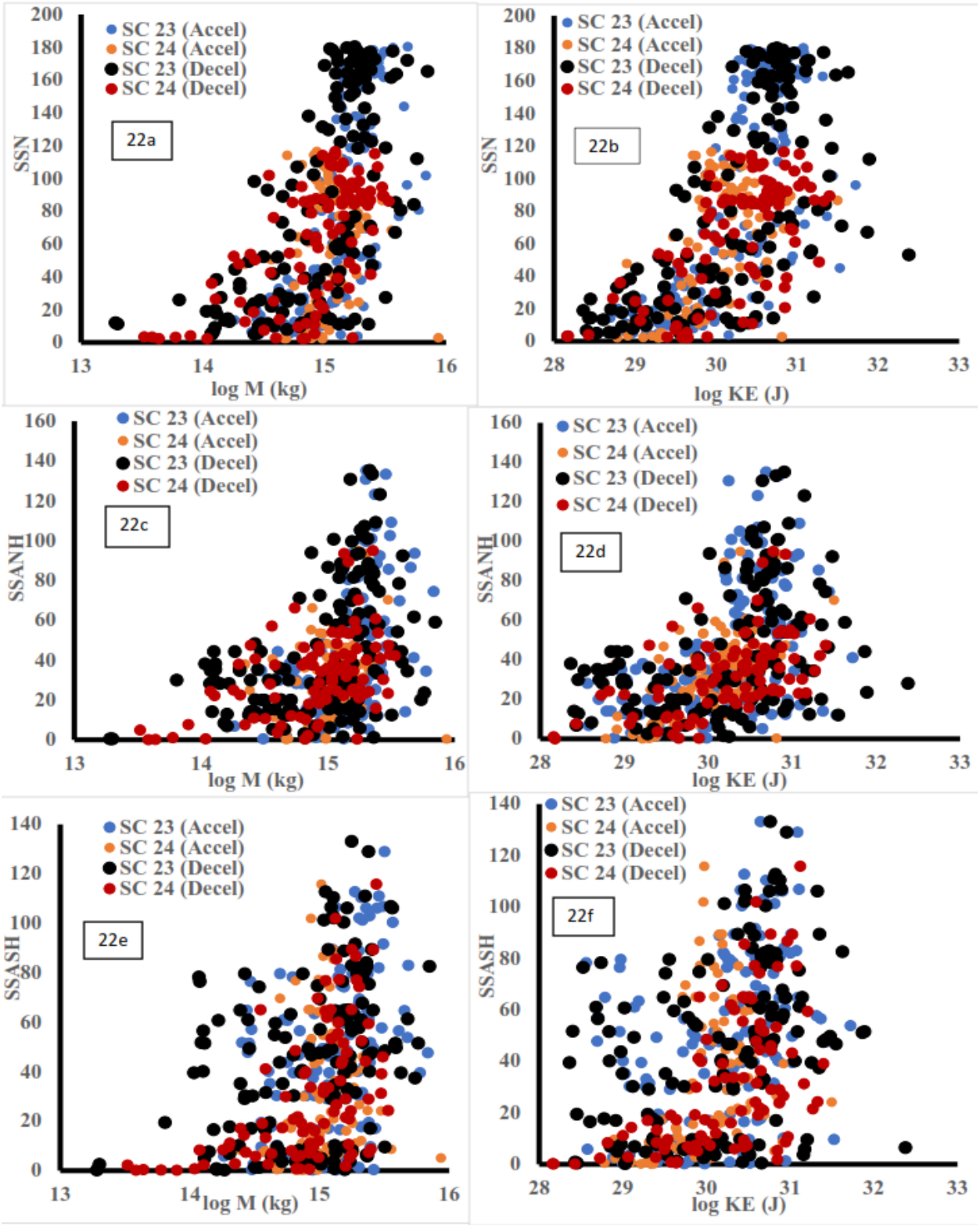

Fig 22: The Scatter Plot of the SSN, SSANH, and SSASH with speed at log M (a, c, e) and log Kinetic Energy (b, d, f) for Accelerated and Decelerated CMEs During SC s 23 and 24, Using the 27-day mean Values

Therefore, the correlation between sunspot numbers or areas and the acceleration or deceleration of CMEs is indirect and mediated by the broader heliospheric environment. There exists a general positive correlation between sunspot activity and the mass and kinetic energy of CMEs during Solar Cycles 23 and 24. However, the relationship is complex, with variations observed between the two cycles and potential hemispheric differences. The acceleration or deceleration of CMEs is primarily influenced by their interaction with the solar wind and interplanetary magnetic fields, rather than directly by sunspot activity. Further research is necessary to elucidate the nuanced interplay between sunspot characteristics and CME dynamics (Mishra et al., 2019; Lamy et al., 2019).

4.5 Regression Analysis of CME Parameters.

Table 3: Correlation Coefficients of CMEs Parameters Estimated Using the 27-day Mean Values

	SC 23	SC 24	SC 23	SC 24
	ACCEL	ACCEL	DECEL	DECEL
	r	r	r	r
LS/20R	0.72	0.07	0.92	0.90
LS/AW	0.55	0.62	0.64	0.75
LS/M	0.73	0.36	0.72	0.57
LS/KE	0.85	0.70	0.81	0.69
20R/AW	0.06	-0.38	0.76	0.83
20R/M	0.40	-0.12	0.79	0.66
20R/KE	0.50	-0.06	0.84	0.75
AW/M	0.67	0.37	0.72	0.74
AW/20R	0.72	0.62	0.72	0.77
M/KE	0.90	0.80	0.95	0.94

Table 3 shows the correlation coefficient amongst the parameters of accelerating and decelerating CMEs in SCs 23 and 24. For decelerating CMEs, there is a consistently moderate to strong correlation between the parameters studied with generally $r \geq 0.6$.

For accelerated CMEs, during SC 23, there is a strong correlation between LS and speed at 20R but no correlation during SC 24. The AW and speed at 20R do not correlate during SC 23 but showed some anti-correlation during SC 24. The mass/kinetic energy shows no correlation in accelerated CME during SC 24, but some form of positive correlation during SC 23.

Linear speeds are measured assuming a constant velocity during the early phase of the CME's motion, while the speed at 20R is computed as the change in distance over time near the 20 solar radii point. The correlation between the linear speed of CMEs and their speed at 20R has been studied extensively in solar physics. Research generally shows a positive correlation, meaning that faster CMEs tend to maintain their speed as they propagate outward, though the relationship may not always be perfectly linear due to factors such as solar wind interactions and CME acceleration or deceleration. CMEs with higher linear speeds tend to have higher speeds at 20R. This trend is consistent with the idea that the initial kinetic energy of a CME largely determines its propagation characteristics in the early phase, but the correlation can also be influenced by the interaction of

the CME with the surrounding solar wind, where faster CMEs are more likely to decelerate due to drag forces, while slower CMEs may accelerate (Sheeley et al., 1999; Gopalswamy et al., 2001, Yashiro et al., 2004). These studies collectively reinforce that while a correlation exists, CME dynamics are complex and depend on various factors, including the initial launch conditions and interactions with the interplanetary medium.

CONCLUSION:

This study presents a detailed comparative analysis of accelerating and decelerating CMEs during SCs 23 and 24. Using CME parameters derived from LASCO data (Howard and Tappin, 2009) and solar activity metrics such as SSA and SSN (Ramesh, 2010), key findings include: Decelerating CMEs show stronger correlations with SSA and SSN during SC 23, likely due to higher levels of solar activity and more significant aerodynamic drag effects (Cargill, 2004). This relationship weakens in SC 24, reflecting reduced solar activity.

CMEs are critical drivers of space weather and are strongly influenced by the solar activity cycle. The relationship between CME parameters (linear speed (LS), speed at 20 solar radii (20R), angular width (AW), mass (M), and kinetic energy (KE)) and solar activity indicators (sunspot numbers (SSN) and sunspot areas in the Northern (SSANH) and Southern hemispheres (SSASH), during SCs 23 and 24, has been studied.

A positive correlation exists between the LS and the speed at 20 solar radii of CMEs, particularly for faster CMEs that are decelerating. This correlation reflects the initial kinetic energy imparted during the CME eruption. However, slower CMEs often experience acceleration, while faster ones tend to decelerate due to drag forces in the solar wind (Gopalswamy et al., 2015). CME angular width shows a moderate but positive correlation with solar activity for both accelerating and decelerating CMEs for the two SCs. Halo CMEs have been excluded from our analysis of CME ejection directions due to the use of the Central Position Angle (CPA) parameter in this study instead of the Mean Position Angle (MPA). However, this exclusion is not expected to significantly diminish their overall influence, as halo CMEs were included in the analysis of other CME parameters. Halo CMEs are known to be indicators of energetic CMEs, occurring more frequently during solar maximum and being strongly associated with higher-energy events (Yashiro et al., 2004). Accelerated and decelerated CME mass and kinetic energy are highly correlated with sunspot activity, peaking during solar maxima. Larger sunspot areas often correspond to higher-energy CMEs due to the intense magnetic field complexity (Vršnak et al., 2010). Studies reveal a hemispheric asymmetry in sunspot numbers and areas, with one hemisphere dominating activity in a given solar cycle. This asymmetry affects CME productivity and characteristics. For instance, the Northern Hemisphere was more active during the early phases of SC 24, while the Southern Hemisphere dominated during its declining phase (Temmer et al., 2006). Thus, CMEs originating in the hemisphere with greater sunspot activity tend to have higher speeds and kinetic energy. This correlation aligns with the magnetic flux available for CME eruptions in active regions.

SC 23 exhibited stronger solar activity, higher sunspot numbers, and more energetic CMEs compared to the weaker Solar Cycle 24. This difference is reflected in the average linear speed, angular width, and kinetic energy of CMEs, which were lower during Cycle 24 (Gopalswamy et al., 2015). These studies highlight the intricate relationships between accelerating and decelerating CME parameters and solar activity, emphasizing the influence of solar cycle strength and hemispheric asymmetry on CME dynamics

These findings underscore the importance of differentiating between accelerating and decelerating CMEs when assessing their propagation behavior and their relationships with solar activity. The observed variability across cycles contributes to refining CME propagation models, which are essential for improving space weather forecasts and mitigating impacts on Earth's technological infrastructure and human activities. Future work should explore these relationships in Solar Cycle 25, building upon predictions from recent studies (Penza et al., 2023) to understand whether reduced solar activity trends persist and their potential implications for CME dynamics.

Disclaimer (Artificial intelligence)

Option 1:

Author(s) hereby declare that NO generative AI technologies such as Large Language Models (ChatGPT, COPILOT, etc.) and text-to-image generators have been used during the writing or editing of this manuscript.

REFERENCES

1. Bartels, J. (1934). Twenty-seven-day recurrences in terrestrial-magnetic and solar activity, 1923–1933. *Terrestrial Magnetism and Atmospheric Electricity*, *39*(3), 201–202.storms.Journal of Geophysical Research: Space Physics 105(A4), 7491-7508.
2. Bazilevskaya, G., Broomhall, M. A., Elsworth, Y., & Nakariakov, V. M. (2014). A combined analysis of the observational aspects of quasi-biennial oscillation in solar magnetic activities. *Space Science Reviews*, *186*(1-4), 359-386. https://doi.org/10.1007/s11214-014-0068-0
3. Cane, H. V., Richardson, I. G., & St. Cyr, O. C. (2010). A study of solar energetic particle events in relation to coronal mass ejections. *Journal of Geophysical Research: Space Physics*, *115*(A8), A08101. https://doi.org/10.1029/2009JA014848
4. Cargill, P. J. (2004). "On the Aerodynamic Drag Force Acting on Interplanetary Coronal Mass Ejections". *Solar Physics*, 221(1), 135-149. doi:10.1023/B.0000033366.10725.
5. Chatfield, C. (2003). *The analysis of time series: An introduction* (6th ed.). Chapman and Hall/CRC.

6. Chen, J. (2011). Coronal mass ejections: Models and their observational basis. *Living Reviews in Solar Physics, 8*(1), 1. https://doi.org/10.12942/lrsp-2011-1
7. Chen, X., Wang, H., & Zhou, X. (2020). Statistical models for analyzing time series data. *Journal of Statistical Methods*, 45(2), 113–128. https://doi.org/10.xxxx
8. Chowdhury, P., Choudhary, D. P., & Gosain, S. (2013). Study of North–South asymmetry in solar activity during solar cycles 23 and 24. The Astrophysical Journal, 768(2), 188. https://doi.org/10.1088/0004-637X/768/2/188
9. Clette, F., & Lefèvre, L. (2012). Are the sunspots really vanishing? Anomalies in solar cycle 23 and implications for long-term models and proxies. *Journal of Space Weather and Space Climate, 2*(A06), 1–12. https://doi.org/10.1051/swsc/2012004
10. Cremades, H., & Bothmer, V. (2004). On the three-dimensional configuration of coronal mass ejections." Astronomy & Astrophysics, 422(1), 307-322.
11. Du, Z. L. (2012). Correlations between CME parameters and sunspot activity. *Solar Physics*, 278(1), 121–129.
12. Forbes, T. G. (2000) A review on coronal mass ejections." *Journal of Geophysical Research: Space Physics*, 105(A10), 23153–23166.
13. Gautam, S. P., Adhikari, L., Zank, G. P., Silwal, A., and Zhao, L., (2024), Solar Cycle Dependence of the Turbulence Cascade Rate at 1 au The Astrophysical Journal, 968:12 (9pp), **DOI** 10.3847/1538-4357/ad4797
14. Gautam, S.P., Silwal, A., Bashyal, A. *et al.* Tracking IMF Fluctuations Nearby Sun Using Wavelet Analysis: Parker Solar Probe First Encounter Data. *Geomagn. Aeron.* **62**, 138–150 (2022). https://doi.org/10.1134/S0016793222020074
15. Georgoulis, M. K., Nindos, A., & Zhang, H. (2019). The source and engine of coronal mass ejections. Philosophical Transactions of the Royal Society A: Mathematical, Physical and Engineering Sciences, 377(2148), 20180094. https://doi.org/10.1098/rsta.2018.0094
16. Gopalswamy, N., Mäkelä, P., Yashiro, S., & Akiyama, S. (2018). Extreme space weather events in solar cycle 24 associated with major eruptive events in solar cycle 23. *Earth, Planets and Space, 70*, 42. https://doi.org/10.1186/s40623-017-0653-zGopalswamy, N., & Yashiro, S. (2005). Properties of accelerating and decelerating CMEs. Space Science Reviews, 123(1-3), 135-176. https://doi.org/10.1007/s11214-005-1385-8
17. Gopalswamy, N., & Yashiro, S. (2006). Coronal mass ejections and associated phenomena. *Space Science Reviews, 123*(1-3), 159–177. https://doi.org/10.1007/s11214-006-9016-8
18. Gopalswamy, N., Yashiro, S., & Michalek, G**.** (2015). Kinetic energy of CMEs in Solar Cycles 23 and 24. *Journal of Geophysical Research: Space Physics*, 120(7), 5263-5272. https://doi.org/10.1002/2015JA021446
19. Gopalswamy, N., Yashiro, S., Michalek, G., et al. (2001). Relation between CME speed and flare energy release. *Journal of Geophysical Research: Space Physics*, *106*(A12), 29207–29217. https://doi.org/10.1029/2001JA000065
20. Gopalswamy, N., Yashiro, S., Michalek, G., Stenborg, G., Vourlidas, A., Freeland, S., & Howard, R. (2009). Coronal mass ejections and other extreme characteristics of the 2006 December solar eruptions. Journal of Geophysical Research: Space Physics, 114(A11), A00A22. Doi: 10.1029/2009JA014175
21. Hamilton, J. D. (1994). *Time series analysis*. Princeton University Press.

22. Howard, T. A., & Tappin, S. J. (2009). Interplanetary coronal mass ejection observed in the heliosphere: 1. Review of theory. Space Science Reviews, 147, 31-54. https://doi.org/10.1007/s11214-009-9542-5
23. Hundhausen, A. J. (1997). "Coronal Mass Ejections." In J. R. Jokipii, C. P. Sonett, & M. S. Giampapa (Eds.), Cosmic Winds and the Heliosphere. University of Arizona Press.
24. Kahler, S. (1987). Coronal mass ejections. Reviews of Geophysics, 25(3), 663-675. https://doi.org/10.1029/RG025i003p00663
25. Kahler, S. W. (2006). Coronal mass ejections and solar energetic particles. Space Science Reviews, 123(1-3), 35-38.
26. Koenker, R. (2005). *Quantile regression*. Cambridge University Press.
27. Lamy, P., Floyd, O., Boclet, B., & Gilardy, H. (2019). Coronal mass ejections over solar cycles 23 and 24. *Space Science Reviews*, 215(5), 39.
28. Li, K. J., Gao, P. X., Zhan, L. S., Shi, X. J., & Zhu, W. W. (2008). The hemispheric sunspot numbers in the descending phase of solar cycle 23. Solar Physics, 245(1), 269-278. https://doi.org/10.1007/s11207-007-9049-1
29. Li, X., & Luhmann, J. G. (2013). Distribution of CMEs with different angular widths and comparison with the phase of sunspot number in the 23rd solar cycle. *Chinese Journal of Space Science*, 33(3), 225–230.
30. Liu, Y. D., Luhmann, J. G., Kajdič, P., Kilpua, E. K. J., Lugaz, N., Nitta, N. V., ... & Bale, S. D. (2016). Observations of an extreme storm in interplanetary space caused by successive coronal mass ejections. *Nature Communications*, 7, 13104.
31. Lugaz, N., Vourlidas, A., Roussev, I. I., & Morgan, H. (2012). Determining the azimuthal properties of coronal mass ejections from multi-spacecraft observations. The Astrophysical Journal, 759(2), 68. Doi: 10.1088/0004-637X/759/2/68
32. Manchester, W. B., Kilpua, E. K. J., Liu, Y. D., Lugaz, N., Riley, P., Török, T., & Vršnak, B. (2017). The physical processes of CME/ICME evolution. *Space Science Reviews*, 212, 1159–1219.
33. Mishra, W., Srivastava, N., & Chakrabarty, D. (2019). Evolution of coronal mass ejections in the interplanetary medium: An integrated approach. *Astrophysics and Space Science*, 364(4), 61. https://doi.org/10.1007/s10509-019-3532-1
34. Möstl, C., Rollett, T., Frahm, R. A., Liu, Y., Long, D. M., Colaninno, R. C., … & Farrugia, C. J. (2012). Multi-point shock and flux rope analysis of the 2010 April 5-6 coronal mass ejection. The Astrophysical Journal, 758(2), 10. Doi: 10.1088/0004-637X/758/2/10
35. Onuchukwu C. C and Umuogbana A. O. (2024). Comparative Analysis of Coronal Mass Ejections (CMEs) Across Solar Cycles 23 And 24. A J Planetary Space Sci 3(3): 136 DOI**: https://doi.org/10.36266/AJPSS/136**
36. Penza, V., Luca, B., Cantoresi, M., Criscuoli, S., & Berrilli, F. (2023). *Prediction of Solar Cycle 25: Application and Comparison*. *Frontiers in Italian Studies on Space Weather and Space Climate*. https://doi.org/10.1007/s12210-023-01184-y
37. Pesnell, W. D. (2016). Predictions of solar cycle 24: How are we doing? *Space Weather, 14*(1), 10–21. https://doi.org/10.1002/2015SW001304
38. Petrovay, K. (2020). Solar cycle prediction. Living Reviews in Solar Physics, 17(2). https://doi.org/10.1007/s41116-020-0022-x

39. Ramesh, K. B. (2010). Coronal mass ejections and sunspots – Solar cycle perspective. The Astrophysical Journal Letters, 712(1), L77-L80. https://doi.org/10.1088/2041-8205/712/1/L77
40. Ramesh, K. B. and Rohini, V. S., (2008), Coronal Background X-Ray Emission And The Associated Indicators Of Photospheric Magnetic Activity. The Astrophysical Journal, 686: L41–L44, 1–8
41. Richardson, I. G., Cane, H. V., & Cliver, E. W. (2016). The relationship between solar activity and geomagnetic storms driven by coronal mass ejections over four solar cycles. *Journal of Space Weather and Space Climate, 6*, A1. https://doi.org/10.1051/swsc/2016001
42. Rousseeuw, P. J., & Leroy, A. M. (2003). *Robust regression and outlier detection*. Wiley.
43. Schrijver, C. J., & DeRosa, M. L. (2003). Photospheric and heliospheric magnetic fields. Solar Physics, 212(1), 165-200.
44. Schwenn, R., Dal Lago, A., Huttunen, E., & Gonzalez, W. D. (2005). The association of coronal mass ejections with their effects on the terrestrial environment. Annales Geophysicae, 23(3), 1033-1059. Doi: 10.5194/angeo-23-1033-2005
45. Sheeley, N. R., Walters, J. H., Wang, Y. M., & Howard, R. A. (1999). Continuous tracking of coronal outflows: Two kinds of coronal mass ejections. Journal of Geophysical Research: Space Physics, 104(A11), 24739-24768. https://doi.org/10.1029/1999JA900308
46. Sheeley, N. R., Walters, J. H., Wang, Y.-M., & Howard, R. A. (1997). Continuous tracking of coronal outflows: Two kinds of coronal mass ejections. *The Astrophysical Journal*, 484(2), 472–478.
47. Shen, F., Wu, S. T., Feng, X., & Wu, C. C. (2012). Acceleration and deceleration of coronal mass ejections during propagation and interaction. *Journal of Geophysical Research: Space Physics, 117*(A11), A11101. https://doi.org/10.1029/2012JA017776
48. Silwal, A., Gautam, P. S., Chaudhary, K., Khanal, M., Joshi, S., Dangaura, S., Adhikari, B., (2021) Study of Solar Wind Parameters During Geomagnetic Storm of 26th August 2018 and 28th September 2017, Thai Journal of Physics Vol. 38 No. 2 54-68
49. Singh, Y. P., & Bhargawa, M. (2017). Characteristics of sunspot cycles and prediction of solar cycle 25 amplitude. Journal of Astrophysics and Astronomy, 38(1), 11. https://doi.org/10.1007/s12036-017-9442-4
50. Solanki, S. K. (2003). Sunspots: An overview. Astronomy and Astrophysics Review, 11(2-3), 153-286. https://doi.org/10.1007/s00159-003-0018-4
51. Temmer, M., Veronig, A. M., Vr, P., & erka, J. (2008). Temporal aspects and frequency distributions of solar flares. The Astrophysical Journal, 673(2), L95.
52. Uga, C. I., Gautam, S. P., Seba, E. B. (2024) TEC disturbances caused by CME-triggered geomagnetic storm of September 6–9, 2017, Heliyon, Volume 10, Issue 10, e30725
53. Vourlidas, A., Howard, R. A., Esfandiari, E., Patsourakos, S., Yashiro, S., & Michalek, G. (2010). Comprehensive analysis of CME mass and energy properties over a full solar cycle. *The Astrophysical Journal*, *722*(2), 1522-1538. https://doi.org/10.1088/0004-637X/722/2/1522
54. Vršnak, B. (2001). Dynamics of solar coronal eruptions. *Journal of Geophysical Research: Space Physics, 106*(A11), 25249–25260. https://doi.org/10.1029/2000JA004007

55. Vršnak, B., & Žic, T. (2007). Transit times of interplanetary coronal mass ejections and the solar wind speed. Astronomy & Astrophysics, 472(3), 937-943. https://doi.org/10.1051/0004-6361:20077499
56. Webb, D. F., & Howard, R. A. (2012). Coronal mass ejections: Observations. Living Reviews in Solar Physics, 9(1), 3.
57. Webb, D. F., Cliver, E. W., Crooker, N. U., St. Cyr, O. C., & Thompson, B. J. (2000). Relationship of halo coronal mass ejections, magnetic clouds, and magnetic
58. Wilcox, R. R. (2017). *Introduction to robust estimation and hypothesis testing* (4th ed.). Academic Press.
59. Winter, L. M., & Balasubramaniam, K. S. (2016). Solar Cycle 23 and 24 Coronal Mass Ejection Rates and the Relationship to Sunspot Number. *Space Weather*, 14(5), 273–285. https://doi.org/10.1002/2015SW001313
60. Witten, I. H., Frank, E., & Hall, M. A. (2016). *Data mining: Practical machine learning tools and techniques* (4th ed.). Morgan Kaufmann.
61. Yashiro, S., Gopalswamy, N., Michalek, G., et al. (2004). A catalog of white light coronal mass ejections observed by the SOHO spacecraft. *Journal of Geophysical Research: Space Physics*, *109*(A7), A07105. https://doi.org/10.1029/2003JA010282
62. Zhang, J., & Dere, K. P. (2006). A statistical study of main and secondary helical magnetic fields in coronal mass ejections. The Astrophysical Journal, 649(1), 452-461. Doi: 10.1086/505736
63. Zhang, Y., & Liu, J. (2017). Correlation between angular widths of CMEs and characteristics of their solar source regions. *The Astrophysical Journal*, 849(2), 79.